ARTICLE

Corrected: Publisher Correction

https://doi.org/10.1038/s41586-019-1156-9

Innervation of thermogenic adipose tissue via a calsyntenin 3β–S100b axis

Xing Zeng[1,2], Mengchen Ye[3], Jon M. Resch[4], Mark P. Jedrychowski[1,2], Bo Hu[1,2], Bradford B. Lowell[4,5], David D. Ginty[3] & Bruce M. Spiegelman[1,2]*

The sympathetic nervous system drives brown and beige adipocyte thermogenesis through the release of noradrenaline from local axons. However, the molecular basis of higher levels of sympathetic innervation of thermogenic fat, compared to white fat, has remained unknown. Here we show that thermogenic adipocytes express a previously unknown, mammal-specific protein of the endoplasmic reticulum that we term calsyntenin 3β. Genetic loss or gain of expression of calsyntenin 3β in adipocytes reduces or enhances functional sympathetic innervation, respectively, in adipose tissue. Ablation of calsyntenin 3β predisposes mice on a high-fat diet to obesity. Mechanistically, calsyntenin 3β promotes endoplasmic-reticulum localization and secretion of S100b—a protein that lacks a signal peptide—from brown adipocytes. S100b stimulates neurite outgrowth from sympathetic neurons in vitro. A deficiency of S100b phenocopies deficiency of calsyntenin 3β, and forced expression of S100b in brown adipocytes rescues the defective sympathetic innervation that is caused by ablation of calsyntenin 3β. Our data reveal a mammal-specific mechanism of communication between thermogenic adipocytes and sympathetic neurons.

A hallmark of mammalian evolution is the emergence of brown adipose tissue (BAT), an organ that is specialized for performing non-shivering thermogenesis[1]. The presence of BAT confers an evolutionary advantage to mammals by enhancing their adaptability to cold stress and the survival of newborns. The powerful ability of thermogenic fat to oxidize substrates and increase energy expenditure has drawn growing interest as a therapeutic approach to address obesity and associated metabolic disorders[2].

BAT thermogenesis requires innervation by the sympathetic nervous system. Sympathetic nerves release the neurotransmitter noradrenaline from local axons[3,4], which activates the β-adrenergic receptor–cAMP–PKA pathway in adipocytes to drive lipolysis and thermogenic respiration[5,6]. Consistent with the thermogenic function of BAT, this tissue is much more richly innervated by sympathetic nerves than white adipose tissue (WAT)[7]. Nevertheless, the molecular basis of this selective recruitment of sympathetic innervation has remained largely unexplored.

PRDM16 has recently been identified as an important transcriptional regulator that drives the thermogenic program in beige adipocytes[8,9], which are a distinct type of inducible thermogenic adipocytes that mainly reside in subcutaneous WAT[10]. Forced expression of PRDM16 leads to increased sympathetic innervation of beige adipocytes[11]; and adipose-specific ablation of PRDM16 has the opposite effect[12]. These observations strongly suggest that adipocyte-derived factors can influence the extent of sympathetic innervation of the adipose tissue. Here we show that a previously unknown, mammal-specific membrane protein, which we have named calsyntenin 3β (CLSTN3β), promotes the sympathetic innervation of both brown and beige adipocytes. CLSTN3β binds to—and enhances the protein expression and secretion of—S100b, a protein that is unconventionally secreted without a signal peptide. S100b, in turn, acts as a neurotrophic factor to stimulate sympathetic axon growth.

Clstn3b is an adipose-specific gene

Adipose-specific ablation of lysine-specific demethylase 1 (*Lsd1*, also known as *Kdm1a*) has previously been found to cause severe BAT dysfunction[13]. Expression of calsyntenin 3 (*Clstn3*) is strongly downregulated in LSD1-deficient BAT (Extended Data Fig. 1a). CLSTN3 is a plasma-membrane protein that promotes synaptogenesis in the central nervous system[14]. In contrast to the known form of *Clstn3*, the completely distinct and unannotated form of *Clstn3b* is expressed in BAT (Fig. 1a). *Clstn3b* appears to contain three exons: the first exon, which is large and unique, lies within an intron of *Clstn3*, and the final two exons are shared with *Clstn3* (Fig. 1a). Chromatin immunoprecipitation with sequencing (ChIP–seq) analyses for histone markers and transcription regulators suggest that a promoter and enhancer of *Clstn3b* that are distinct from those of *Clstn3* exist in BAT (Extended Data Fig. 1b). Taken together, these observations suggest that *Clstn3b* is a previously unknown gene that is expressed in BAT, rather than a splicing variant of *Clstn3*.

Clstn3b mRNA expression is highly restricted to adipose tissue: the level of expression in the interscapular BAT is sixfold higher than in either the inguinal subcutaneous WAT or the perigonadal visceral WAT (Fig. 1b). *Clstn3b* expression is strongly induced in the inguinal subcutaneous WAT upon exposure to cold (Extended Data Fig. 1c), which suggests that *Clstn3b* is also highly expressed in beige adipocytes.

We next attempted to clone the *Clstn3b* cDNA. We successfully amplified a 1,074-bp open reading frame that was predicted to encode a protein of 357 amino acids in length, from a cDNA library of mouse BAT (Fig. 1c); this confirmed the existence of *Clstn3b* at the transcript level. Notably, the N-terminal extracellular portion of CLSTN3—which is essential for interaction between CLSTN3 and α-neurexins, and for the synaptogenic activity of this protein—is completely missing in CLSTN3β, which strongly suggests that the two proteins have distinct functions.

[1]Department of Cancer Biology, Dana Farber Cancer Institute, Boston, MA, USA. [2]Department of Cell Biology, Harvard Medical School, Boston, MA, USA. [3]Department of Neurobiology, Howard Hughes Medical Institute, Harvard Medical School, Boston, MA, USA. [4]Division of Endocrinology, Diabetes and Metabolism, Department of Medicine, Beth Israel Deaconess Medical Center, Harvard Medical School, Boston, MA, USA. [5]Program in Neuroscience, Harvard Medical School, Boston, MA, USA. *e-mail: bruce_spiegelman@dfci.harvard.edu

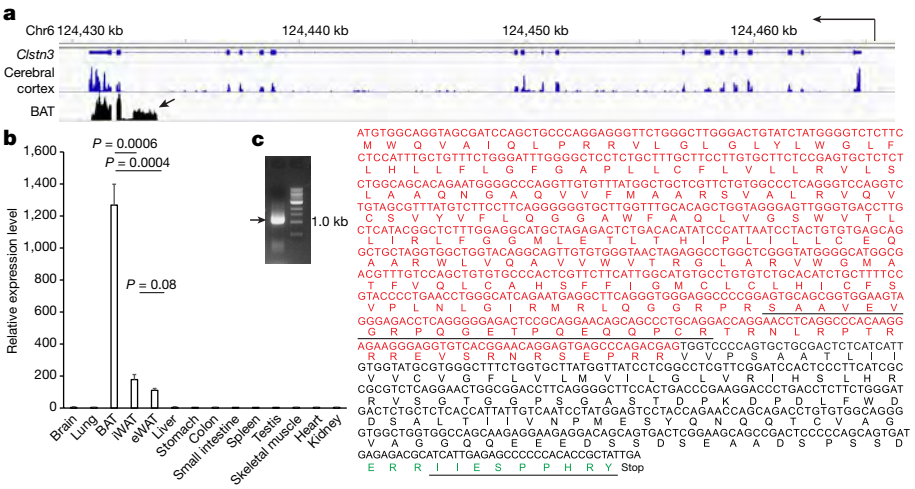

Fig. 1 | *Clstn3b* encodes an adipocyte-specific protein. a, Distribution of RNA sequencing reads at the *Clstn3* locus, from BAT and cerebral cortex. The arrow denotes the exon that is unique to *Clstn3b*. **b**, Tissue specificity of *Clstn3b* expression as determined by quantitative PCR ($n = 3$ mice). eWAT, epididymal WAT; iWAT, inguinal WAT. **c**, Cloning of *Clstn3b* from a BAT cDNA library. Red denotes nucleotides and amino acids derived from the unique exon of *Clstn3b*. The underlined region denotes peptides that were detected by mass spectrometry. Green denotes the peptide used to generate the CLSTN3β antibody. Data are mean ± s.e.m. and analysed by unpaired Student's two-sided *t*-test.

To detect CLSTN3β at the protein level, we developed a rabbit polyclonal antibody against a C-terminal peptide of CLSTN3β (amino acids shown in green in Fig. 1c). The antibody detected a doublet band of the expected size for the full-length protein in BAT (Extended Data Fig. 1d). We immunoprecipitated endogenous CLSTN3β with this antibody, and mass spectrometry analysis identified two peptides that were consistent with the predicted sequence; one derived from the region shared with *Clstn3* and the other derived from the unique exon that was not included in the mouse protein database (corresponding to the underlined amino acids in Fig. 1c, Extended Data Fig. 1d), which thus provided definitive evidence at the peptide level for the existence of CLSTN3β.

We next examined the evolution of *Clstn3b*. Unequivocal homologues can be identified only in mammals that give birth to live progeny (Extended Data Fig. 1e). A fragment with limited homology, but which is unproductive in terms of protein coding, exists in an intron of *Clstn1* of the Chinese softshell turtle (Extended Data Fig. 1f), which suggests *Clstn3b* evolved in mammals after their divergence from reptiles. By contrast, *Clstn3* is conserved throughout the entire vertebrate family.

CLSTN3β localizes to the endoplasmic reticulum

We first studied the function of CLSTN3β by determining its subcellular localization. Ectopically expressed CLSTN3β in primary brown adipocytes was found to co-localize with KDEL, which is a marker for the endoplasmic reticulum; this suggests that CLSTN3β localizes to the endoplasmic reticulum (Fig. 2a). Endogenous CLSTN3β was detected as more-weakly stained puncta that were also positive for KDEL (Fig. 2b). To visualize the subcellular localization of CLSTN3β at the ultrastructural level, we expressed an APEX2 reporter fused to the C terminus of CLSTN3β in brown adipocytes; APEX2 localization based on 3,3′-diaminobenzidine tetrahydrochloride reactivity was then examined by electron microscopy. Consistent with the immunofluorescence data, APEX2 strongly labelled the endoplasmic reticulum (Fig. 2c). By contrast, we observed no APEX2 labelling of other membranous organelles (Extended Data Fig. 2a, b). The endoplasmic-reticulum localization of CLSTN3β was further supported by BAT fractionation and western blot analysis (Extended Data Fig. 2c).

CLSTN3β promotes adipose thermogenesis

To study the function of CLSTN3β in adipose thermogenesis and whole-body energy metabolism, we generated a global *Clstn3b*-knockout mouse strain. Deletion of *Clstn3b* was verified by DNA sequencing, quantitative PCR, western blot and immunofluorescence (Extended Data Fig. 3a–d). Expression and splicing of *Clstn3* is unaffected in *Clstn3b*-knockout mice (Extended Data Fig. 3e). On a chow diet, the body weights of *Clstn3b*-knockout mice were not significantly different from wild-type mice, but *Clstn3b*-knockout mice had significantly higher body-fat mass (Extended Data Fig. 3f, g). Histological analysis and triglyceride quantification showed that CLSTN3β-deficient

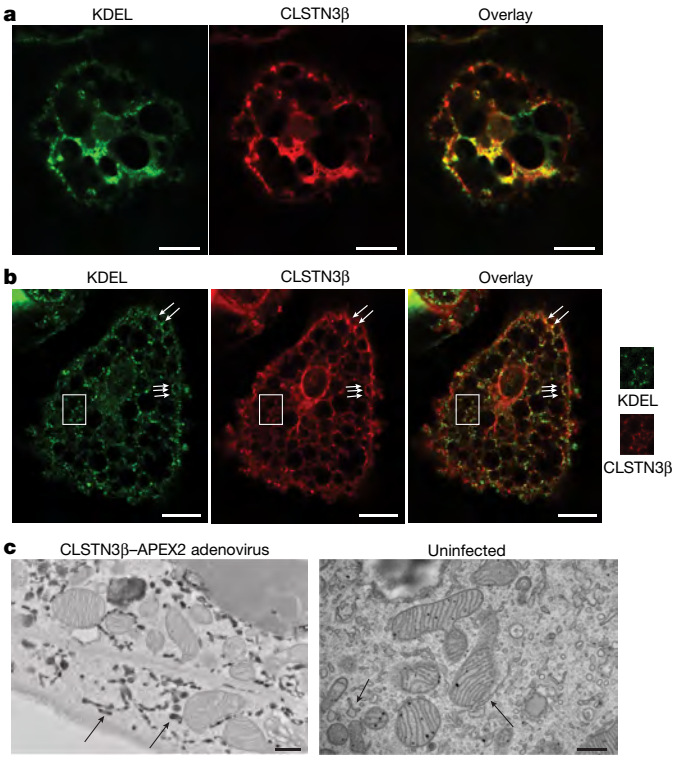

Fig. 2 | CLSTN3β localizes to the endoplasmic reticulum. **a**, **b**, Immunofluorescence analysis of localization of ectopically expressed (**a**) or endogenous (**b**) CLSTN3β in primary brown adipocytes. Green, KDEL; red, CLSTN3β. Arrows denote puncta specific for CLSTN3β. In **b**, the region inside the white box is enlarged for clearer view. **c**, Electron microscopy analysis of the localization of CLSTN3β–APEX2. Arrows denote endoplasmic reticulum that is positive or negative for APEX2 in infected or uninfected cells, respectively. Scale bars, 10 μm (**a**, **b**), 500 nm (**c**).

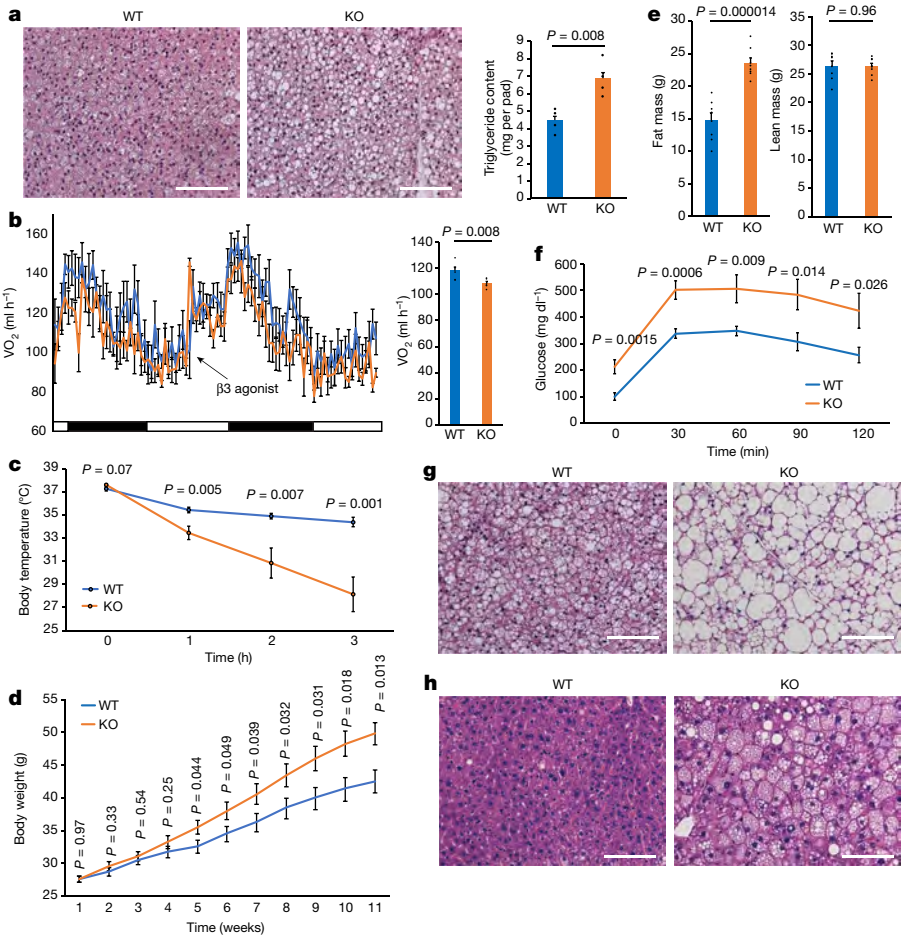

Fig. 3 | Ablation of *Clstn3b* impairs adipose thermogenesis. a, Histology and triglyceride quantification of wild-type (WT) and *Clstn3b*-knockout (KO) BAT ($n = 4$ mice). **b**, Indirect calorimetry analysis of wild-type and *Clstn3b*-knockout mice ($n = 6$ mice). **c**, Cold tolerance test of wild-type and *Clstn3b*-knockout mice ($n = 6$ mice). **d**–**f**, Body-weight curve (**d**), body composition ($n = 8$ mice) (**e**) and glucose tolerance test ($n = 7$ mice) (**f**) of wild-type and *Clstn3b*-knockout mice on high-fat diet. **g**, **h**, Histology of BAT (**g**) and liver (**h**) of wild-type and *Clstn3b*-knockout mice on high-fat diet. Scale bars, 100 μm. Data are mean ± s.e.m. and analysed by unpaired Student's two-sided *t*-test.

BAT has significantly more lipid deposition than wild-type BAT; this parameter often reflects BAT dysfunction (Fig. 3a). An indirect calorimetry study showed that *Clstn3b*-knockout mice had lower rates of O_2 consumption and CO_2 production than wild-type mice (Fig. 3b, Extended Data Fig. 3h), although their food intake and physical activity were unaltered (Extended Data Fig. 3i, j). The acute respiratory response to an injection with the β3-adrenergic agonist CL-316,243 was similar between wild-type and knockout mice (Fig. 3b, Extended Data Fig. 3k).

To directly assess adaptive thermogenesis, we performed a cold tolerance test and found knockout mice were notably more cold-sensitive than wild-type mice (Fig. 3c), which provides strong evidence that *Clstn3b*-knockout mice have defective adaptive thermogenesis. Together, these findings suggest that the *Clstn3b*-knockout mice are defective in energy expenditure and adaptive thermogenesis compared to wild-type mice, which is consistent with these knockout mice displaying BAT dysfunction. However, *Clstn3b* deletion does not seem to affect the BAT response to pharmacological β3-adrenergic stimulation.

To understand the role of CLSTN3β in diet-induced obesity, we challenged the mice with a high-fat diet; *Clstn3b*-knockout mice gained weight more rapidly than wild-type mice on this diet (Fig. 3d). Body composition analyses revealed that knockout mice had a higher fat mass than wild-type mice, but mice of both genotypes had comparable lean masses (Fig. 3e). The knockout mice also showed significantly increased levels of fasting blood glucose, strongly impaired glucose tolerance, more lipid accumulation in BAT and increased liver steatosis (Fig. 3f–h). These results indicate that *Clstn3b*-knockout mice are more susceptible to diet-induced obesity and glucose intolerance than wild-type mice.

To complement the loss-of-function model of *Clstn3b*, we generated an adipose-specific *Clstn3b*-transgenic model and performed the same set of analyses as described above. The transgenic mice displayed a phenotype that was opposite to that of the knockout mice in all of the assays (Fig. 4a–h, Extended Data Fig. 4a–h). These data provide strong support for a pro-thermogenic function of CLSTN3β.

CLSTN3β enhances sympathetic innervation

The observation that both *Clstn3b*-knockout and -transgenic mice showed altered cold sensitivity—coupled with their normal responses to the β3-adrenergic agonist—suggested that CLSTN3β may affect sympathetic innervation of adipose tissue. Indeed, we observed no significant difference in noradrenaline-induced respiration between wild-type or knockout brown adipocytes (Fig. 5a), which suggests that the phenotype at the organismal level cannot be explained by alterations in the intrinsic thermogenic capacity of brown adipocytes.

To assess BAT sympathetic innervation, we performed tyrosine hydroxylase immunostaining. Notably, tyrosine hydroxylase immunoreactivity of the knockout BAT was substantially reduced relative to the wild type (Fig. 5b). Immunostaining of TUBB3, a neural-specific tubulin, yielded similar results (Fig. 5b). These results indicate that knockout BAT has reduced growth of sympathetic nerves, relative to wild type. Decreased expression of several thermogenesis-related genes in knockout BAT was observed upon acute cold exposure following pre-acclimatization at thermoneutrality, which is consistent with

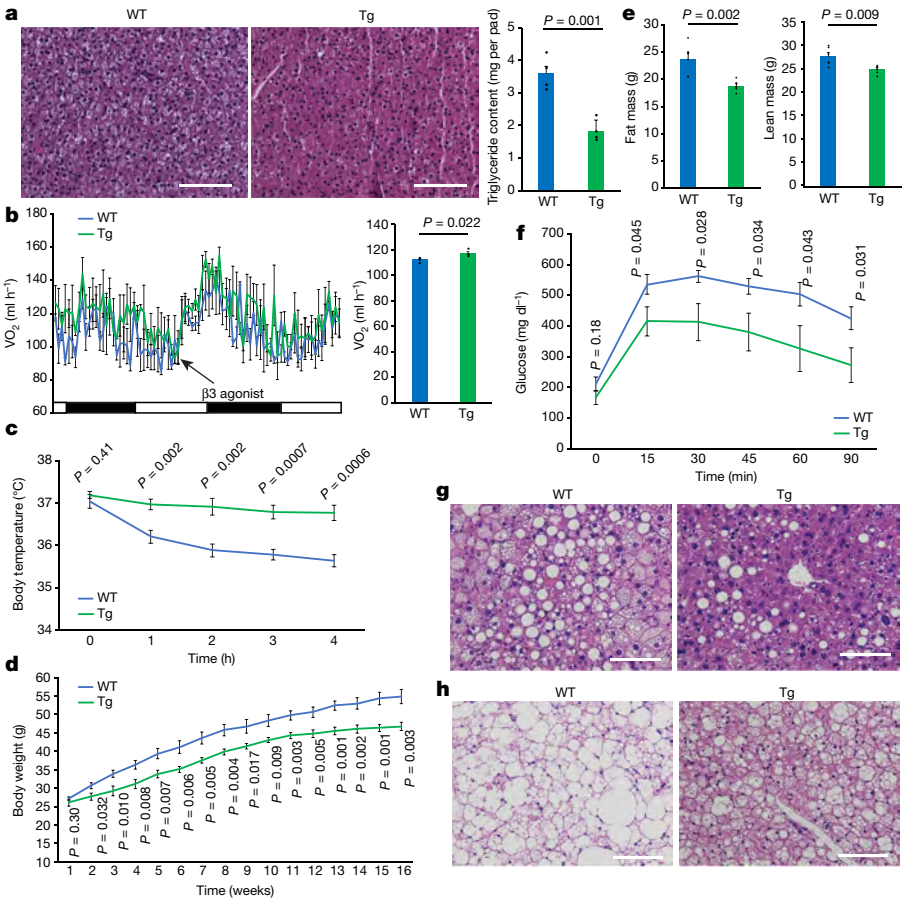

Fig. 4 | Transgenic expression of CLSTN3β enhances adipose thermogenesis. a, Histology and triglyceride quantification of wild-type and *Clstn3b*-transgenic (Tg) BAT ($n = 4$ mice). **b**, Indirect calorimetry analysis of wild-type and *Clstn3b*-transgenic mice ($n = 4$ mice). **c**, Cold tolerance test of wild-type and *Clstn3b*-transgenic mice ($n = 6$ mice). **d**–**f**, Body-weight curve (**d**), body composition (**e**) and glucose tolerance test ($n = 6$ mice) (**f**) of wild-type and *Clstn3b*-transgenic mice on high-fat diet. **g**, **h**, Histology of BAT (**g**) and liver (**h**) of wild-type and *Clstn3b*-transgenic mice on high-fat diet. Scale bars, 100 μm. Data are mean ± s.e.m. and analysed by unpaired Student's two-sided *t*-test.

reduced sympathetic innervation (Extended Data Fig. 5a). BAT from *Clstn3b*-transgenic mice showed enhanced sympathetic innervation (Fig. 5c), which provides further support for the notion that CLSTN3β promotes BAT thermogenesis by enhancing sympathetic innervation.

To assess whether the BAT innervation and the thermogenic defects of the global *Clstn3b*-knockout mice reflect the deletion of *Clstn3b* from adipocytes, we restored CLSTN3β expression specifically in brown adipocytes by crossing the *Clstn3b*-knockout mice to an *Adipoq-cre* line, and injecting the Cre-dependent adeno-associated virus (AAV) AAV-Clstn3b into the BAT[15]. Cre^+ BAT with restored CLSTN3β expression showed significantly reduced lipid deposition and increased sympathetic innervation, compared with Cre^- BAT (Fig. 5d, e). The Cre^+ mice also showed significantly improved cold tolerance and increased energy expenditure compared with Cre^- mice (Fig. 5f, Extended Data Fig. 5b). These data show that restoring CLSTN3β expression specifically in brown adipocytes is sufficient to rescue the defects of the global *Clstn3b*-knockout mice.

We next asked whether CLSTN3β is important for sympathetic innervation of beige adipocytes. Similar to BAT, inguinal subcutaneous WAT from wild-type mice that were acclimatized at 4 °C for 1 week exhibited more-extensive sympathetic axons than WAT from knockout mice exposed to similar conditions (Extended Data Fig. 5c); this suggests that CLSTN3β has an important role in promoting sympathetic innervation of beige adipocytes, as well as in the classical BAT.

To investigate the functional importance of CLSTN3β to sympathetic innervation of BAT, we chemogenetically activated sympathetic premotor neurons, and assessed the downstream BAT response. Previous studies have identified medullary raphe neurons that express vesicular glutamate transporter 3 (VGLUT3), which are proposed to activate BAT thermogenesis via direct projections to preganglionic sympathetic neurons in the spinal cord[16]. We crossed the *Slc17a8-ires-cre* (*Slc17a8* is also known as *Vglut3*) mouse line[17] to *Clstn3b*-knockout and -transgenic lines, and stereotaxically injected Cre-dependent AAV-hM3Dq-mCherry or AAV-mCherry into the medullary raphe region of the brain stem to drive stable expression of the transgene specifically in the neurons that express VGLUT3. Injection of clozapine-*N*-oxide (CNO; a ligand of hM3Dq), but not of saline, into mice that received AAV-hM3Dq-mCherry induced FOS expression in the medullary raphe region, as well as an increase of 0.9 °C in interscapular temperature (Fig. 5g). CNO injection into mice that received AAV-mCherry produced neither FOS expression nor a temperature response (Fig. 5g), which confirmed that CNO specifically activates sympathetic premotor neurons in the medullary raphe region to trigger the thermogenic response.

We next examined the response of *Clstn3b*-knockout and -transgenic mice to CNO. The response was reduced from 0.9 °C in wild-type mice to 0.3 °C in knockout mice, but increased from 0.6 °C in control mice to 1.2 °C in transgenic mice (Fig. 5h–i). Taken together, these findings indicate that ablation of *Clstn3b* impairs the functional sympathetic innervation of thermogenic adipose tissue, whereas transgenic expression has the opposite effect.

CLSTN3β promotes the secretion of S100b

Our findings raised the critical question of how an intracellular membrane protein might regulate sympathetic innervation of thermogenic adipocytes. To gain insight into this question, we performed quantitative

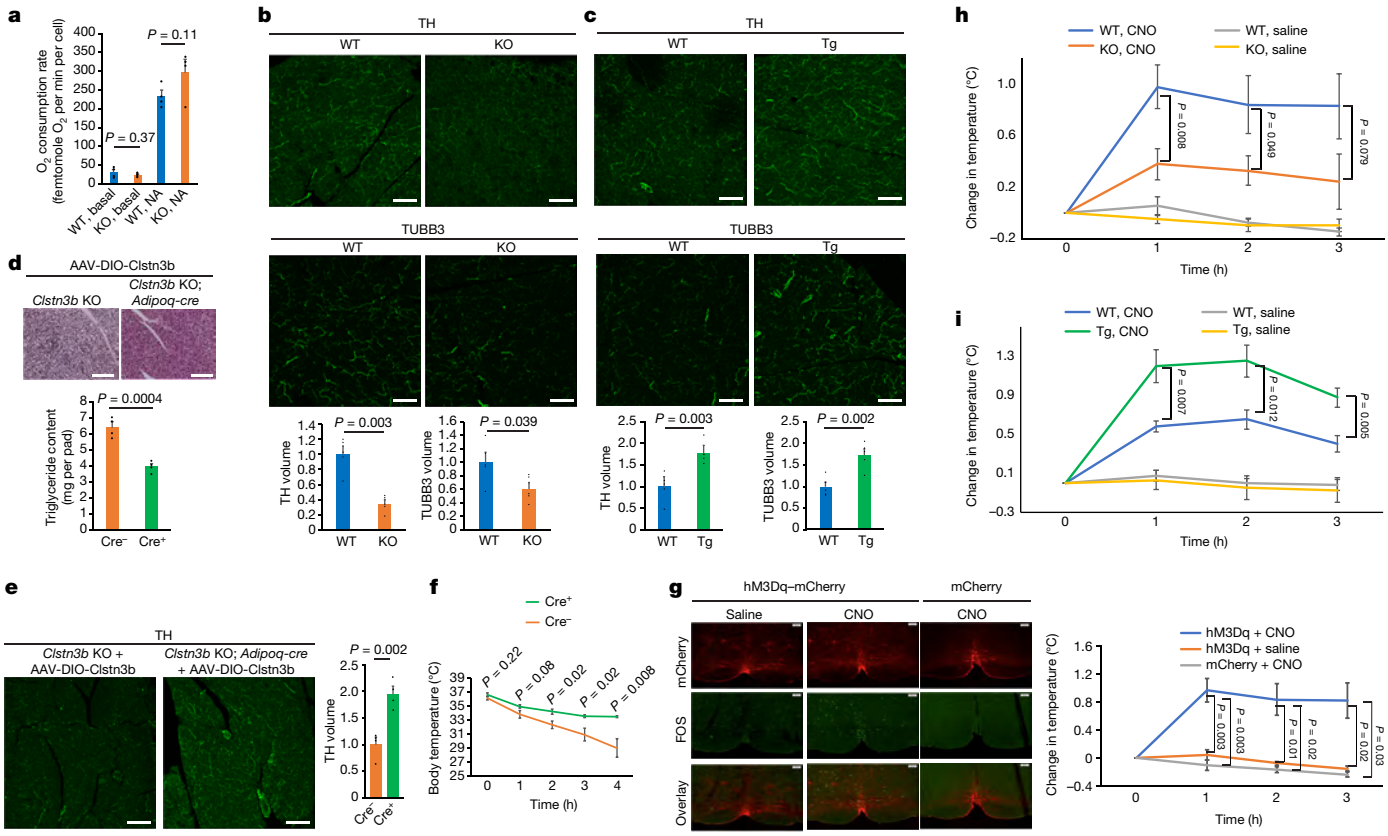

Fig. 5 | CLSTN3β promotes functional sympathetic innervation of the adipose tissues. a, Respiration rates of wild-type or *Clstn3b*-knockout brown adipocytes ($n = 4$ biologically independent samples). NA, noradrenaline. **b**, **c**, Immunostaining of cryo-section of wild-type and *Clstn3b*-knockout BAT (**b**), and wild-type and *Clstn3b*-transgenic BAT (**c**) ($n = 5$ mice). TH, tyrosine hydroxylase. **d**–**f**, Histology and triglyceride quantification (**d**), tyrosine hydroxylase staining (**e**) and cold tolerance test (**f**) of *Clstn3b*-knockout ± *Adipoq-cre* mice, receiving AAV-DIO-Clstn3b ($n = 4$ mice). **g**, FOS immunoreactivity and thermogenic response to CNO administration ($n = 8$ mice for hM3Dq + CNO, $n = 3$ mice for hM3Dq + saline and mCherry + CNO). **h**, **i**, Thermogenic response to CNO administration in wild-type and *Clstn3b*-knockout mice ($n = 8$ mice) (**h**), and wild-type and *Clstn3b*-transgenic mice ($n = 4$ mice) (**i**). Scale bars, 100 μm. Data are mean ± s.e.m. and analysed by unpaired Student's two-sided *t*-test.

whole-tissue proteomic analysis of wild-type and *Clstn3b*-knockout BAT (Fig. 6a, Supplementary Table 1). The most-strongly downregulated (47% down) protein in the knockout BAT was S100b. Previous studies have established that S100b is a protein that is highly expressed by astrocytes in the central nervous system, and that it has neurotrophic activity[18,19]. S100b expression is much higher in BAT than in WAT, and is strongly induced in the inguinal subcutaneous WAT upon exposure to cold (Extended Data Fig. 6a, b). Notably, S100b transcription is positively regulated by PRDM16 (Extended Data Fig. 6c–e). We therefore examined the hypothesis that S100b might be a critical adipocyte-derived neurotrophic factor that promotes sympathetic innervation of adipose tissue.

We first asked whether S100b possesses neurotrophic activity for sympathetic neurons. S100b significantly induced neurite growth from primary sympathetic neurons (Fig. 6b), thus demonstrating that S100b can act as a neurotrophic factor for sympathetic neurons.

We next tested whether forced expression of S100b in brown adipocytes could alleviate the *Clstn3b*-knockout defects, by injecting Cre-dependent AAV-S100b into the BAT of *Clstn3b*-knockout mice with or without *Adipoq-cre*. We observed a significantly reduced triglyceride content and increased sympathetic innervation only in the presence of *Adipoq-cre* (Fig. 6c, d). Moreover, Cre^+ mice showed significantly increased cold tolerance and energy expenditure, compared with Cre^- mice (Fig. 6e, Extended Data Fig. 6f), which indicates that forced S100b expression is sufficient to reverse the innervation and thermogenic defects caused by CLSTN3β deficiency.

We determined whether S100b-deficient BAT phenocopies CLSTN3β-deficient BAT by analysing BAT sympathetic innervation of a global *S100b*-knockout mouse line[20]. S100b-deficient BAT displayed a notable decrease in the level of sympathetic innervation (Fig. 6f), which suggests that S100b could be a target of CLSTN3β that mediates sympathetic-adipose communication. We observed no difference between sympathetic innervation of the salivary gland of wild-type and *S100b*-knockout mice (Extended Data Fig. 6g). Moreover, ablation of *S100b* completely obliterates the ability of *Clstn3b* transgenesis to enhance BAT sympathetic innervation (Fig. 6f), which suggests that S100b works downstream of CLSTN3β. Finally, we mechanistically examined how CLSTN3β deficiency results in a reduction in S100b protein level in BAT. We observed no difference in *S100b* mRNA level between wild-type and *Clstn3b*-knockout BAT (Extended Data Fig. 6h), which suggests that S100b is post-transcriptionally regulated by CLSTN3β. We then cultured primary *Clstn3b*-knockout brown adipocytes, and ectopically expressed S100b with or without CLSTN3β. In these experiments, we observed that CLSTN3β led to a modest increase in cellular level of the S100b protein (Extended Data Fig. 6i). Similar results were obtained when using HEK293T cells (Extended Data Fig. 6j). CLSTN3 did not have such an effect (Extended Data Fig. 6j). Co-expression of CLSTN3β significantly promotes co-localization of S100b with the endoplasmic-reticulum marker KDEL in brown adipocytes (Fig. 6g, h), which suggests that CLSTN3β promotes the association of S100b with the endoplasmic reticulum. The amount of S100b secreted into the medium increased strongly in the presence of CLSTN3β (Fig. 6i), thus indicating that CLSTN3β promotes secretion of S100b. S100b is highly unusual in that it is a secreted protein with no signal peptide; the pathway of its secretion has therefore been unclear. CLSTN3β did not promote secretion of complement factor D (also known as adipsin)

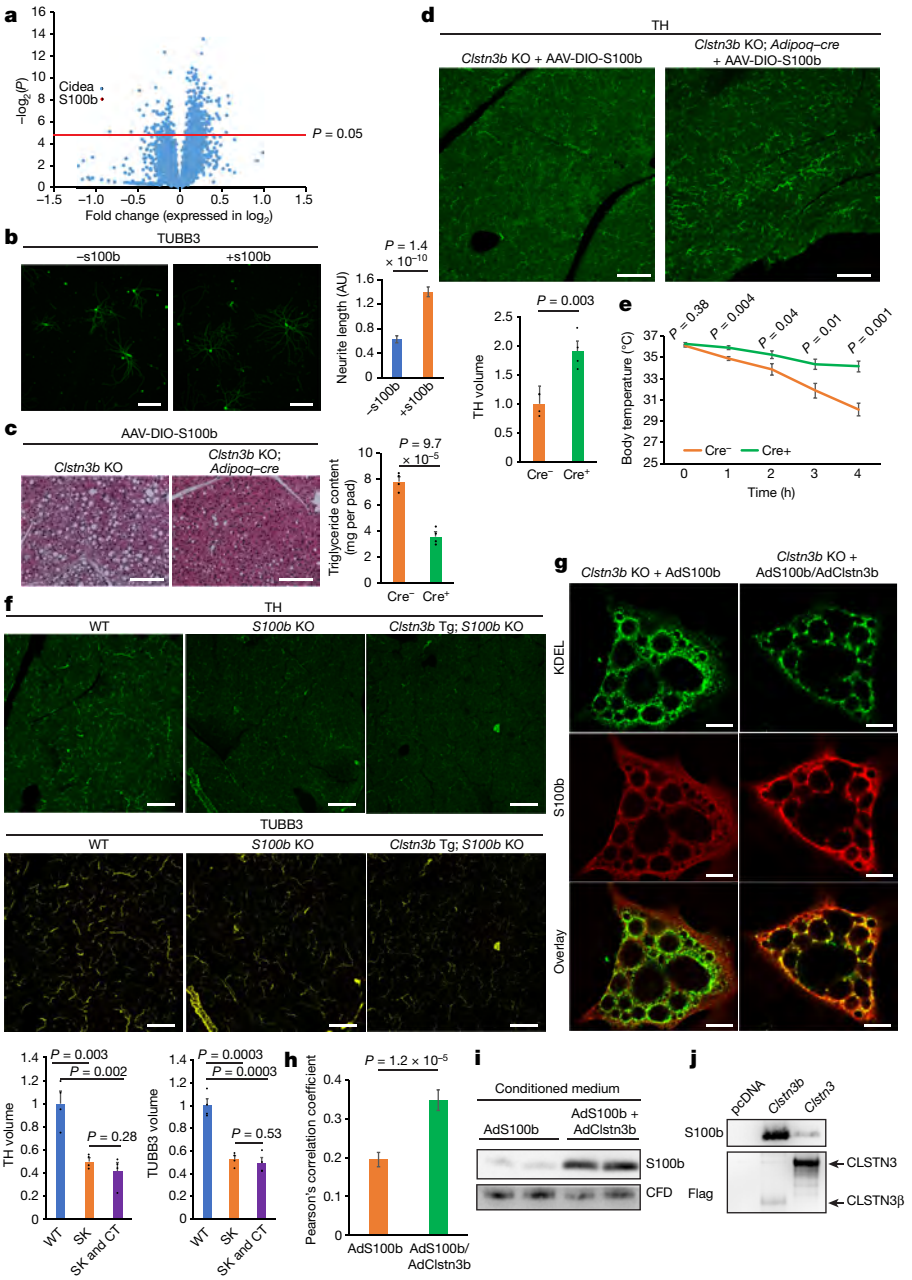

Fig. 6 | CLSTN3β promotes secretion of S100b, an adipocyte-derived neurotrophic factor. a, Proteomics of wild-type and *Clstn3b*-knockout BAT. **b**, TUBB3 immunostaining of sympathetic neurons ± S100b ($n = 25$ cells). AU, arbitrary unit. **c**–**e**, Histology, and triglyceride quantification (**c**), tyrosine hydroxylase staining (**d**) and cold tolerance test (**e**) of *Clstn3b*-knockout ± *Adipoq-cre* mice, receiving AAV-DIO-S100b ($n = 4$ mice). **f**, Tyrosine hydroxylase and TUBB3 immunostaining of BAT from wild-type, *S100b*-knockout, and *Clstn3b*-transgenic and *S100b*-knockout mice ($n = 4$ mice). CT, *Clstn3b* transgenic; SK, *S100b* knockout. **g**, **h**, Immunostaining (**g**) and Pearson's correlation analysis (**h**) of S100b and KDEL in brown adipocytes ($n = 35$ cells). **i**, Western blot analysis of conditioned medium from brown adipocytes. **j**, Binding assay of S100b, and CLSTN3β and CLSTN3. Scale bars, 100 μm. Data are mean ± s.e.m. and analysed by unpaired Student's two-sided *t*-test.

(Fig. 6i, Extended Data Fig. 6k), a secreted protein with a signal peptide that is abundantly expressed in adipocytes.

The observation that CLSTN3β promotes the endoplasmic-reticulum association of S100b suggests that CLSTN3β may directly bind S100b. We found that CLSTN3β bound S100b much more strongly than did CLSTN3 (Fig. 6j). Our data thus suggest that CLSTN3β—but not CLSTN3—may enhance secretion of S100b via direct physical interaction at the endoplasmic reticulum.

Discussion

Innervation by the sympathetic nervous system is important for both the development and activation of brown and—potentially beige—fat[21–24]. Previously, very little has been known about the identity of adipocyte-derived factors that promote the innervation of thermogenic fat. We show here that the newly identified protein CLSTN3β, which is selectively and abundantly expressed in thermogenic adipocytes, is involved in the innervation of thermogenic fat. Genetic ablation of *Clstn3b* leads to a deficiency in adipose innervation and thermogenic function. Human adipose tissue also expresses *Clstn3b* (Extended Data Fig. 7), which suggests CLSTN3β may have a similar role of promoting adipose innervation in humans.

We have shown that CLSTN3β resides mainly in the endoplasmic reticulum but is also involved in innervation. It appears to do so—at least in part—by driving the secretion of S100b, a protein with trophic activity on sympathetic neurons. The secretion pathway of S100b is unclear, as this protein does not have a signal peptide[25]. Our findings

support a chaperone-like activity of CLSTN3β on S100b, which explains why the ablation of *Clstn3b* leads to a reduction in the level of S100b protein in BAT. Understanding the detailed mechanism of non-canonical secretion requires more analysis. However, the notion that S100b is used as a physiological neurotrophic factor is supported by both gain- and loss-of-function evidence. In addition to being regulated at the protein level by CLSTN3β, S100b transcription is positively regulated by PRDM16; this provides an explanation for the altered levels of adipose sympathetic innervation observed in PRDM16 gain- and loss-of-function mouse models[11,12]. CLSTN3β expression is not as sensitive as S100b to changes in PRDM16 levels.

Previous studies have suggested that nerve growth factor (NGF) or brain-derived neurotrophic factor (BDNF) are factors that potentially promote the sympathetic innervation of thermogenic fat[26,27]. Nevertheless, ribosome profiling data driven by adipose-specific Cre revealed extremely low-to-undetectable levels of *Ngf* and *Bdnf* mRNA, which indicates that these factors may not be produced by adipocytes at a physiologically relevant level[28,29]. By contrast, CLSTN3β and S100b are abundantly and selectively expressed in thermogenic adipocytes, which provides strong support for their roles as adipocyte-derived neurotrophic factors. Our data do not exclude the possibility that NGF or BDNF also contribute to adipose innervation.

Our findings should help to advance understandings of the basic biology of thermogenic fat and its innervation. Moreover, the identification of a soluble protein with neurotrophic actions on the sympathetic nervous system may also provide a therapeutic opportunity for promoting thermogenic fat activity in the treatment of obesity and associated metabolic disorders.

Online content

Any methods, additional references, Nature Research reporting summaries, source data, statements of data availability and associated accession codes are available at https://doi.org/10.1038/s41586-019-1156-9.

Received: 26 September 2018; Accepted: 2 April 2019;
Published online 1 May 2019.

1. Cannon, B. & Nedergaard, J. Brown adipose tissue: function and physiological significance. *Physiol. Rev.* **84**, 277–359 (2004).
2. Seale, P. & Lazar, M. A. Brown fat in humans: turning up the heat on obesity. *Diabetes* **58**, 1482–1484 (2009).
3. Morrison, S. F. Central neural control of thermoregulation and brown adipose tissue. *Auton. Neurosci.* **196**, 14–24 (2016).
4. Zeng, W. et al. Sympathetic neuro-adipose connections mediate leptin-driven lipolysis. *Cell* **163**, 84–94 (2015).
5. Fedorenko, A., Lishko, P. V. & Kirichok, Y. Mechanism of fatty-acid-dependent UCP1 uncoupling in brown fat mitochondria. *Cell* **151**, 400–413 (2012).
6. Kazak, L. et al. A creatine-driven substrate cycle enhances energy expenditure and thermogenesis in beige fat. *Cell* **163**, 643–655 (2015).
7. Daniel, H. & Derry, D. M. Criteria for differentiation of brown and white fat in the rat. *Can. J. Physiol. Pharmacol.* **47**, 941–945 (1969).
8. Seale, P. et al. Transcriptional control of brown fat determination by PRDM16. *Cell Metab.* **6**, 38–54 (2007).
9. Cohen, P. et al. Ablation of PRDM16 and beige fat causes metabolic dysfunction and subcutaneous to visceral adipose switch. *Cell* **156**, 304–316 (2013).
10. Wang, W. & Seale, P. Control of brown and beige fat development. *Nat. Rev. Mol. Cell Biol.* **17**, 691–702 (2016).
11. Seale, P. et al. Prdm16 determines the thermogenic program of subcutaneous white adipose tissue in mice. *J. Clin. Invest.* **121**, 96–105 (2011).
12. Chi, J. et al. Three-dimensional adipose tissue imaging reveals regional variation in beige fat biogenesis and PRDM16-dependent sympathetic neurite density. *Cell Metab.* **27**, 226–236 (2018).
13. Zeng, X. et al. Lysine-specific demethylase 1 promotes brown adipose tissue thermogenesis via repressing glucocorticoid activation. *Genes Dev.* **30**, 1822–1836 (2016).
14. Pettem, K. L. et al. The specific α-neurexin interactor calsyntenin-3 promotes excitatory and inhibitory synapse development. *Neuron* **80**, 113–128 (2013).
15. Saunders, A., Johnson, C. A. & Sabatini, B. L. Novel recombinant adeno-associated viruses for Cre activated and inactivated transgene expression in neurons. *Front. Neural Circuits* **6**, 47 (2012).
16. Nakamura, K. et al. Identification of sympathetic premotor neurons in medullary raphe regions mediating fever and other thermoregulatory functions. *J. Neurosci.* **24**, 5370–5380 (2004).
17. Cheng, L. et al. Identification of spinal circuits involved in touch-evoked dynamic mechanical pain. *Nat. Neurosci.* **20**, 804–814 (2017).
18. Reeves, R. H. et al. Astrocytosis and axonal proliferation in the hippocampus of S100b transgenic mice. *Proc. Natl Acad. Sci. USA* **91**, 5359–5363 (1994).
19. Winningham-Major, F., Staecker, J. L., Barger, S. W., Coats, S. & Van Eldik, L. J. Neurite extension and neuronal survival activities of recombinant S100β proteins that differ in the content and position of cysteine residues. *J. Cell Biol.* **109**, 3063–3071 (1989).
20. Nishiyama, H., Knöpfel, T., Endo, S. & Itohara, S. Glial protein S100B modulates long-term neuronal synaptic plasticity. *Proc. Natl Acad. Sci. USA* **99**, 4037–4042 (2002).
21. Steiner, G., Loveland, M. & Schonbaum, E. Effect of denervation on brown adipose tissue metabolism. *Am. J. Physiol.* **218**, 566–570 (1970).
22. Bachman, E. S. et al. βAR signaling required for diet-induced thermogenesis and obesity resistance. *Science* **297**, 843–845 (2002).
23. Dulloo, A. G. & Miller, D. S. Energy balance following sympathetic denervation of brown adipose tissue. *Can. J. Physiol. Pharmacol.* **62**, 235–240 (1984).
24. Cao, Y., Wang, H. & Zeng, W. Whole-tissue 3D imaging reveals intra-adipose sympathetic plasticity regulated by NGF-TrkA signal in cold-induced beiging. *Protein Cell* **9**, 527–539 (2018).
25. Donato, R. et al. S100B's double life: intracellular regulator and extracellular signal. *Biochim. Biophys. Acta* **1793**, 1008–1022 (2009).
26. Nisoli, E., Tonello, C., Benarese, M., Liberini, P. & Carruba, M. O. Expression of nerve growth factor in brown adipose tissue: implications for thermogenesis and obesity. *Endocrinology* **137**, 495–503 (1996).
27. Sornelli, F., Fiore, M., Chaldakov, G. N. & Aloe, L. Adipose tissue-derived nerve growth factor and brain-derived neurotrophic factor: results from experimental stress and diabetes. *Gen. Physiol. Biophys.* **28**, 179–183 (2009).
28. Chen, Y. et al. Crosstalk between KCNK3-mediated ion current and adrenergic signaling regulates adipose thermogenesis and obesity. *Cell* **171**, 836–848.e13 (2017).
29. Long, J. Z. et al. A smooth muscle-like origin for beige adipocytes. *Cell Metab.* **19**, 810–820 (2014).

Acknowledgements We thank Nikon Imaging Center at Harvard Medical School for all imaging studies; RIKEN Institute for sharing the S100b knockout strain; Z. Herbert and the Molecular Biology Core Facilities at Dana Farber Cancer Institute for sequencing studies; the Rodent Histology Core at Harvard Medical School for histology studies; the EM Core at Harvard Medical School for APEX2 imaging studies; the viral core at Children's Hospital Boston for AAV production; the transgenic core at Beth Israel Deaconess Medical Center for generation of mouse models; Y. Zhu for advice on sequencing data analysis. X.Z. was supported by the American Heart Association postdoctoral fellowship. B.H. is a Cancer Research Institute/Leonard Kahn Foundation Fellow. D.D.G. is an investigator of the Howard Hughes Medical Institute. This study was supported by NIH grant DK31405 to B.M.S.

Author contributions X.Z. conceived the project and designed experiments. X.Z., M.Y. and B.H. performed imaging experiments and data analysis. X.Z. and B.H. performed metabolic assays. J.M.R. performed stereotaxical surgeries, viral injections and post hoc histological analysis for the chemogenetic experiment. M.P.J. performed mass spectrometry analysis. B.B.L. supervised the chemogenetic experiments. D.D.G. supervised analysis of sympathetic innervation. B.M.S. supervised the entire project. X.Z. and B.M.S. wrote the manuscript with discussion and contributions from all authors.

Competing interests The authors declare no competing interests.

Additional information
Extended data is available for this paper at https://doi.org/10.1038/s41586-019-1156-9.
Supplementary information is available for this paper at https://doi.org/10.1038/s41586-019-1156-9.
Reprints and permissions information is available at http://www.nature.com/reprints.
Correspondence and requests for materials should be addressed to B.M.S.
Publisher's note: Springer Nature remains neutral with regard to jurisdictional claims in published maps and institutional affiliations.

METHODS

No statistical methods were used to predetermine sample size. Except imaging data analysis, investigators were not blinded to allocation during experiments and outcome assessment.

Mouse strains. *Clstn3b*-knockout mice were generated using the CRISPR–Cas9 technique. Two guide RNAs (CCCCAGCAGGAAGTGTAAACTGG, ATGG CCCCGTGGCTAAGCCCAGG) flanking the unique exon of *Clstn3b* were synthesized by PNA-BIO. They were microinjected with Cas9 enzyme (CP02, PNA-BIO) into fertilized eggs of mice of the C57BL/6 background at the transgenic core of Beth Israel Deaconess Medical Center. F1 progenies were genotyped with the following primers: CTGCAGGGAGAGCAAGGGGTCAG, GACAGTGCTTTCAACAGTGTCCC and CCAGGCAGAAAGACAGGAAGCTTC. The wild-type allele yielded a band of 368 bp and the knockout allele yielded a band of approximately 480 bp. F1 progenies carrying the knockout allele were crossed with C57BL/6 mice purchased from Jackson Laboratory to screen for germline transmission. F2 *Clstn3b*$^{+/-}$ male mice were then crossed with *Clstn3b*$^{+/-}$ to yield *Clstn3b*$^{+/+}$ and *Clstn3b*$^{-/-}$ mice for analyses. To generate CLSTN3β adipose-specific mice, the mouse *Clstn3b* cDNA was cloned into a construct for integration into the *Rosa26* locus as previously described. The construct was linearized with KpnI and microinjected into C57BL/6 embryonic stem cells. Successful integration of the transgene was validated using long-range PCR (5′-forward: CCTAAAGAAGAGGCTGTGCTTTGGG; 5′-reverse: TGGGCTATGAACTAATGACCCCG; 3′-forward: TTGCAGAAGATCTC CCCAACTGGG; 3′-reverse: CAGTGGCTCAACAACACTTGGTC). Positive clones were transferred into pseudo-pregnant albino C57BL/6J mice at the transgenic core of Beth Israel Deaconess Medical Center. F1 chimaeras were screened for the presence of the *Clstn3b* transgene (forward: CCATCAAGCTGATCCGGAACC; reverse: TACAGACCTGGACCCTGAGGG) and positive males were crossed with albino C57BL/6J female mice to screen for germline transmission. F2 progeny that have both the *Clstn3b* transgene and black fur colour were crossed with *Adipoq-cre* mice to generate adipose-specific transgenic mice. The *Adipoq-cre* and *Vglut3-ires-cre* lines were maintained at the animal facility of Beth Israel Deaconess Medical Center. The *S100b*-knockout line was recovered from cryopreservation at RIKEN Institute, and genotyping was performed following the protocol in the original publication[20]. All mice were maintained under a 12 h light/12 h dark cycle at constant temperature (23 °C), unless otherwise specified, with free access to food and water. All animal studies were approved by and in full compliance with the ethical regulation of the Institutional Animal Care and Use Committee of Beth Israel Deaconess Medical Center. Male mice of 8–12 weeks of age were used for experiments. Sample size was chosen based on the literature and results of pilot experiments to ensure statistical significance could be reached. Randomization was not performed because mice were grouped based on genotype.

CLSTN3β antibody. Rabbit polyclonal antibody to CLSTN3β was generated with the C-terminal peptide DSPSSDERRIIESPPHRY with an N-terminal cysteine for conjugation to the carrier protein keyhole limpet haemocyanin, and affinity-purified with the antigenic peptide (New England Peptide; Covance).

Cryo-section immunostaining. Tissue was collected immediately after euthanizing the mice, and fixed with 4% paraformaldehyde overnight. Tissue was then washed with PBS 5 times, for 10 min each time and incubated in PBS with 30% sucrose for 8 h, and then frozen in Tissue-Tek O.C.T. Compound (Sakura Finetek, 4583). Frozen tissue was cut into 30-μm sections on a Leica CM3050 S cryostat. Sections were briefly rinsed with PBS and blocked with PBS/0.3% Triton X-100/5% FBS overnight. Sections were then stained with tyrosine hydroxylase antibody (AB1542, EMD Millipore, 1:200) and TUBB3 antibody (ab52623, Abcam, 1:200) for two days. Sections were washed with PBS/0.03% Triton X-100/5% FBS 5 times, for 1 h each time and then stained with anti-sheep Alexa Fluor 488 (Thermo Fisher, A-11015, 1:500) and anti-rabbit Alexa Fluor 647 (Thermo Fisher, A-21245, 1:500) for 2 days. Sections were washed with PBS/0.3% Triton X-100/5% FBS 5 times, for 1 h each time and then mounted in ProLong Diamond Antifade Mountant (Thermo Fisher, P36965). Images were taken on a Nikon A1R point scanning confocal microscope.

Image analysis. For each animal, at least six sections of adipose tissues were imaged and analysed. Acquired images were first cleaned up in ImageJ (NIH) using the 'despeckle' function and 'background subtraction' function (rolling ball method, radius = 20). Images were then imported into Imaris (Bitplane). Tyrosine hydroxylase or TUBB3 immunohistochemical signals were rendered by the 'surface' function, which draws contour surfaces over the fluorescent signals and extracts 3D models of the raw 3D *z*-stacked images. The volume of the extracted 3D objects generated by the surface function was used as the volume of tyrosine hydroxylase or TUBB3 signal. Signals on and around blood vessels were manually selected and removed from the final quantifications. Volume and intensity measurements of tyrosine hydroxylase or TUBB3 signals were normalized to the volume of the imaging field. In each experiment, the function parameters were kept the same between genotypes. For Pearson's correlation analysis, images were imported into ImageJ. Individual cells were outlined manually and co-localization between KDEL and S100b were assessed by Pearson's correlation coefficient using the Coloc2 plugin. Images were analysed in a blinded manner.

Superior cervical ganglia culture. Superior cervical ganglia were dissected out and placed in Leibovitz's L-15 medium, and then transferred to DMEM/collagenase type 2 (4 mg/ml)/DNase I (1 mg/ml)/BSA (10 mg/ml) and incubated at 37 °C for 20 min. Superior cervical ganglia were then centrifuged down and transferred to DMEM and 3 mg/ml trypsin, and incubated at 37 °C for 15 min. Superior cervical ganglia were then centrifuged down, and triturated in DMEM and 10% FBS to yield single-cell suspensions. Cells were then centrifuged down, resuspended in DMEM and 10% FBS with or without 100 ng/ml S100b protein (Millipore, 559290).

Primary brown adipocyte culture. BAT was dissected, minced and digested with Krebs Ringer Bicarbonate Modified Buffer (120 mM NaCl, 5 mM KCl, 1 mM $MgCl_2$, 1 mM $CaCl_2$, 0.4 mM K_2HPO_4, 10 mM glucose, 15 mM $NaHCO_3$, 20 mM HEPES, pH 7.4, 4% fatty-acid-free BSA) and 2 mg/ml collagenase B (Worthington, CLSAFB) and 1 mg/ml soybean trypsin inhibitor (Worthington, LS003570) for 30 min at 37 °C. The mixture was centrifuged at 30*g* for 10 min, and the infranatant and stromal vascular fraction were removed with a syringe. Adipocytes were washed with DMEM and 10% FBS 3 times and added to a 24-well plate. Each well was filled to the top with DMEM and 10% FBS, and covered with a coverslip pre-coated with poly-lysine and laminin. After overnight incubation at 37 °C, the coverslip was flipped and placed in DMEM and 10% FBS. The cells were then subjected to adenoviral infection and imaging studies.

APEX2 electron microscopy imaging. CLSTN3β–APEX2 localization was detected by electron microscopy as previously described[30]. In brief, cells that express CLSTN3β–APEX2 were fixed and incubated in a Tris buffer containing diaminobenzidine (DAB, 0.7 mg/ml) and H_2O_2 (0.7 mg/ml) (Sigma, D4293) for 15 min, or until the cytoplasm developed the brown reaction product. After extensive washing, samples were post-fixed with 1% osmium tetroxide, dehydrated and embedded in EPON resin. Forty-eight hours later, coverslips were removed and areas containing cells were randomly selected and mounted. Ultrathin sections (70 nm) were cut and examined on a JOEL electron microscope.

Stereotaxic surgery and viral injections. For viral injections into the medullary raphe, six-to-eight-week-old male mice were anaesthetized with a ketamine (100 mg kg^{-1}) and xylazine (10 mg kg^{-1}) cocktail diluted in 0.9% saline and placed into a stereotaxic apparatus (David Kopf model 940). An incision was made to expose the skull and a small hole was drilled 5.9 mm posterior and 0 mm medial/lateral from bregma. A pulled glass micropipette (20–40-μm diameter tip) was used for stereotaxic injections of AAV. Three injections, 6.0 mm ventral to bregma, and at medial/lateral −0.15 mm, 0 mm and 0.15 mm, were used to target the medullary raphe. Virus was injected (15 nl per injection) by an air pressure system using picolitre air puffs through a solenoid valve (Clippard EV 24VDC), pulsed by a Grass S48 stimulator to control injection speed (20 nl min^{-1}). The pipette was removed 1 min after each injection and, upon completion of the final injection, the incision was closed using Vetbond tissue adhesive (3M). Subcutaneous injection of sustained release meloxicam (4 mg kg^{-1}) was provided as postoperative care. Chemogenetic experiments used AAV8-hSyn-DIO-hM3Dq-mCherry packaged at the Boston Children's Hospital Viral Core (Addgene plasmid 44361; donating investigator, B. Roth). Animals were allowed to recover from stereotaxic surgery for a minimum of 21 days before initiation of any experiments. Following each experimental procedure, the accuracy of AAV injections was confirmed via post hoc histological analysis of mCherry fluorescent protein reporters. All subjects that were determined to be surgical 'misses' on the basis of little or absent reporter expression were removed from analyses.

Histology. Mice were terminally anaesthetized with 7% choral hydrate (500 mg kg^{-1}; Sigma Aldrich) diluted in saline, and transcardially perfused first with 0.1 M phosphate-buffered saline (PBS) and then with 10% neutral-buffered formalin solution (NBF) (Thermo Fisher Scientific). Brains were extracted and post-fixed overnight at 4 °C in NBF. The next day, brains were switched to PBS containing 20% sucrose for cryoprotection. Finally, brains were sectioned coronally at 30 μm on a freezing microtome (Leica Biosystems), and stored in cryoprotectant solution at −20 °C until used for immunofluorescence. For immunofluorescence, brain tissue sections were washed 3× in PBS before a blocking step containing 3% normal donkey serum and 0.4% Triton X-100 in PBS for 1 h at room temperature. Primary antibody was prepared in the same blocking solution and incubated overnight at the following concentrations: rat anti-mCherry (Life Technologies, M11217) 1:3,000, rabbit anti-FOS (EMD Millipore, ABE457) 1:3,000. The next day sections were washed 5× in PBS, then incubated for 2 h at room temperature in Alexa Fluor fluorescent secondary antibody (Life Technologies; 1:1,000) prepared in blocking solution. Finally, sections were washed 3× in PBS, mounted on gelatin-coated slides and coverslipped with Vectashield mounting medium containing DAPI (Vector Labs). Fluorescent images were captured using an Olympus VS120 slide-scanning microscope.

Chemogenetic activation of BAT assay. To monitor BAT response in real time, temperature probes (Bio Medic Data Systems, IPTT-300) were implanted into the interscapular region of mice and temperature was read with a transponder (Bio Medic Data Systems, DAS-7007R). To activate sympathetic neurons, mice were intraperitoneally injected with saline or CNO (Sigma, C0832) at 1 mg/kg.

BAT fractionation and CLSTN3β isolation. BAT fractionation was performed based on a previously described procedure[31]. In brief, whole BAT was dissected and homogenized in a dounce homogenizer in 10 ml of 20 mM HEPES, 1 mM EDTA, 250 mM sucrose, pH 7.4 (HES buffer). The homogenate was filtered with two layers of cheesecloth and centrifuged at 16,000*g* for 15 min. The fat layer was removed and the supernatant (S1) was saved. The pellet (P1) was resuspended in 5 ml HES and applied on top of a 1.12 M sucrose cushion that contained 20 mM HEPES, 1 mM EDTA, pH 7.4, and was centrifuged at 101,000*g* for 70 min to yield a pellet (P2) and fluffy material at the interface (plasma-membrane fraction). P2 was resuspended in 5 ml HES, and centrifuged at 700*g* to yield the nuclei pellet; the supernatant was centrifuged again at 8,000*g* to yield the mitochondria pellet. S1 was centrifuged at 212,000*g* for 70 min to yield the microsome pellet, and the supernatant was the cytosol fraction. To isolate endogenous CLSTN3β, the microsome pellet was solubilized in IP buffer (25 mM HEPES, 150 mM NaCl, 1 mM EDTA, 1% IGEPAL CA-630, 5% glycerol, pH 7.4) and incubated with Dynabeads protein G, pre-loaded with CLSTN3β antibody at 4 °C for 2 h. The beads were washed with IP buffer 3 times, for 5 min each time and incubated with IP buffer containing 100 μg/ml antigenic peptide at 4 °C for 30 min.

AAV injection. Six-week-old male mice were anaesthetized with isoflurane and an incision was made above the interscapular area to expose the underlying adipose tissue. About 3×10^{11} AAV particles were injected into each BAT lobe and the incision was closed with suture. Mice received one injection of meloxicam (2 mg/kg) 24 h before surgery, and another injection immediately after surgery. Mice were allowed to recover for three weeks before analysis. AAV8-EF1a-DIO-Clstn3b or AAV8-EF1a-DIO-S100b were packaged at the Boston Children's Hospital Viral Core (Addgene plasmid 27056; donating investigator, K. Deisseroth).

Cold tolerance assay. Mice were pre-acclimatized at thermoneutrality (28–30 °C) for two weeks and then shifted to 4 °C. Body temperature was measured with a rectal probe (Physitemp, RET3) and a reader (Physitemp, BAT-12).

S100b assays. To detect binding between S100b and CLSTN3β or CLSTN3, HEK293T cells transfected with pcDNA, pcDNA-Clstn3b-Flag or pcDNA-Clstn3-Flag were homogenized with IP buffer (25 mM HEPES 150 mM NaCl, 1 mM $CaCl_2$, 1% lauryl maltose–neopentyl glycol, 5% glycerol, pH 7.4) and centrifuged at 16,000*g* for 10 min. The supernatant was incubated with anti-Flag M2 resin (Sigma, A2220) at 4 °C for 1 h, and the resin was washed with binding buffer (same as IP buffer except lauryl maltose–neopentyl glycol concentration was reduced to 0.02%) 3 times, for 5 min each time. The resin was then incubated with 10 μg/ml recombinant S100b (R&D Systems, 1820-SB-050) in binding buffer at 4 °C for 30 min and then washed with binding buffer 3 times, for 5 min each time. Bound proteins were eluted with 150 μg/ml 3× Flag peptide (Sigma, F4799) in binding buffer at 4 °C for 30 min. To assess S100b secretion, medium was collected from cells that express S100b and centrifuged at 16,000*g* for 20 min. The supernatant was subjected to S100b quantification with an enzyme-linked immunosorbent assay kit (Millipore, EZHS100B-33K). S100b antibody (Abcam, ab51642) was used for immunofluorescence and western blot analysis. The HEK293T cell line used in these experiments was purchased from ATCC and maintained in the Spiegelman laboratory. This cell line has been routinely tested negative for mycoplasma. Authentication of this cell line was not performed for this study.

Quantitative PCR. The following primers were used for quantitative PCR analysis of gene expression. *Clstn3b* fwd, CTCCGCAGGAACAGCAGCCC; rev, AGGATAACCATAAGCACCAG; *S100b* fwd, TGGTTGCCCTCATTGATGTCT; rev, CCCATCCCCATCTTCGTCC. Primers for other genes have previously been described[13].

ChIP–seq and metabolic assays. All ChIP and metabolic experiments were performed as previously described[13].

Whole-mount immunofluorescence. The whole-mount immunostaining of subcutaneous inguinal WAT was performed as previously described[12]. The inguinal, rather than the dorsolumbar, region was selected for imaging.

Mass spectrometry analysis. Quantitative whole tissue proteomics analysis was performed as previously described[13].

Statistics and reproducibility. All experiments have been successfully repeated with similar results for at least three times.

Reporting summary. Further information on research design is available in the Nature Research Reporting Summary linked to this paper.

Data availability

Histone modification marker and transcription factor ChIP–seq datasets generated in this study are available at NIH Sequence Read Archive under the accession code PRJNA526243. Any other relevant data are available from the corresponding author upon reasonable request.

30. Lam, S. S. et al. Directed evolution of APEX2 for electron microscopy and proximity labeling. *Nat. Methods* **12**, 51–54 (2015).
31. Simpson, I. A. et al. Insulin-stimulated translocation of glucose transporters in the isolated rat adipose cells: characterization of subcellular fractions. *Biochim. Biophys. Acta* **763**, 393–407 (1983).

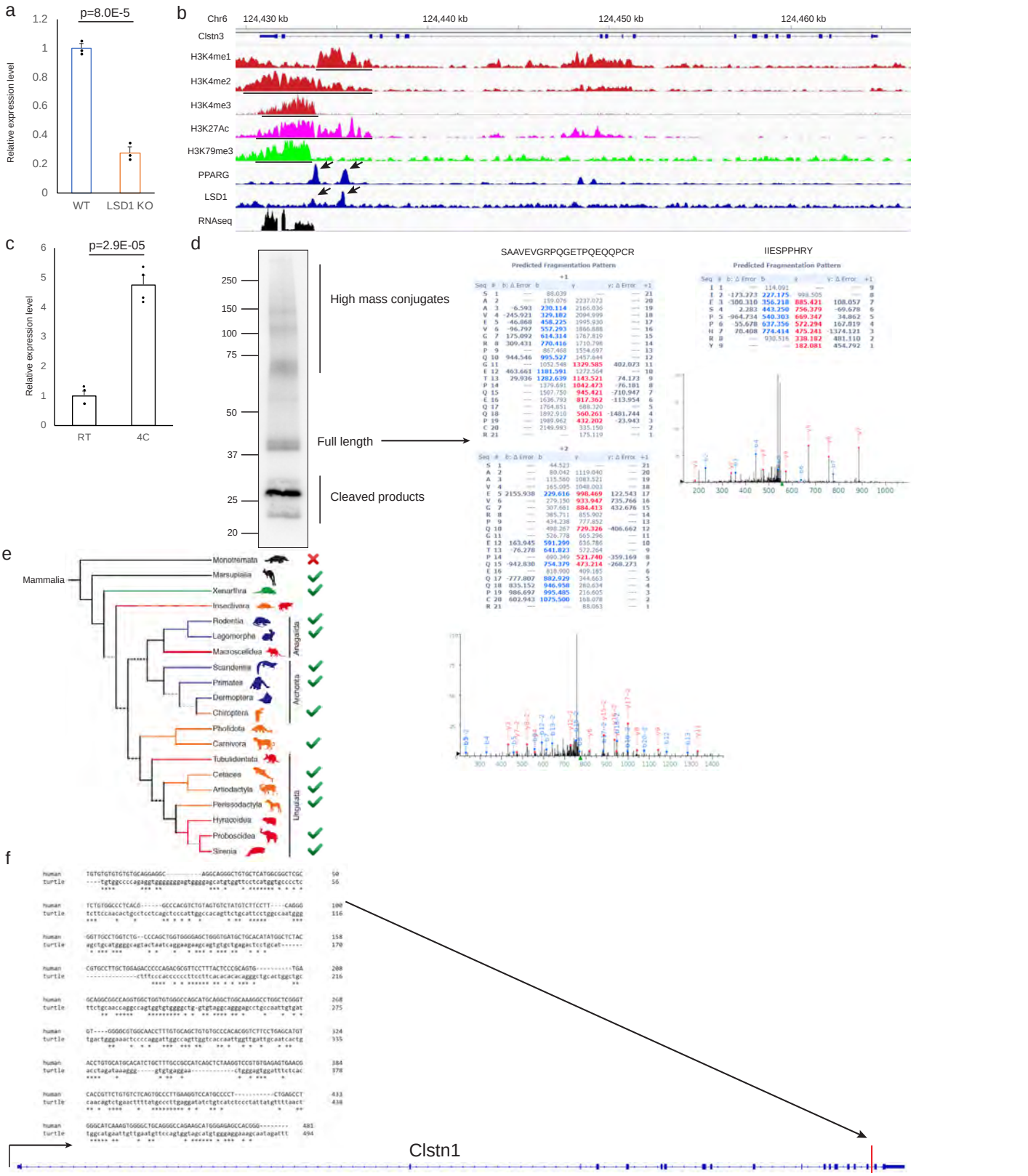

Extended Data Fig. 1 | *Clstn3b* encodes an adipocyte-specific protein. **a**, Quantitative PCR analysis of *Clstn3b* expression in wild-type and *Lsd1*-knockout BAT ($n = 3$ mice). **b**, Histone marker and transcription regulator ChIP–seq at the *Clstn3* locus from BAT. **c**, Quantitative PCR analysis of *Clstn3b* expression in inguinal subcutaneous WAT from mice acclimatized to room temperature or 4 °C ($n = 4$ mice). **d**, Mass spectrometry identification of CLSTN3β peptides. **e**, Conservation of CLSTN3β within the mammalian class. The red cross and green ticks indicates the absence and presence, respectively, of homologues of CLSTN3β in mammalian subclasses. **f**, Sequence alignment between the unique exon of *Clstn3b* from human, and a fragment, in an intron upstream of the penultimate exon of *Clstn1*, in the genome of Chinese softshell turtle. Note how the position of this fragment corresponds to the β-selective exon in *Clstn3*. All data are mean ± s.e.m. Statistical significance was calculated by unpaired Student's two-sided *t*-test.

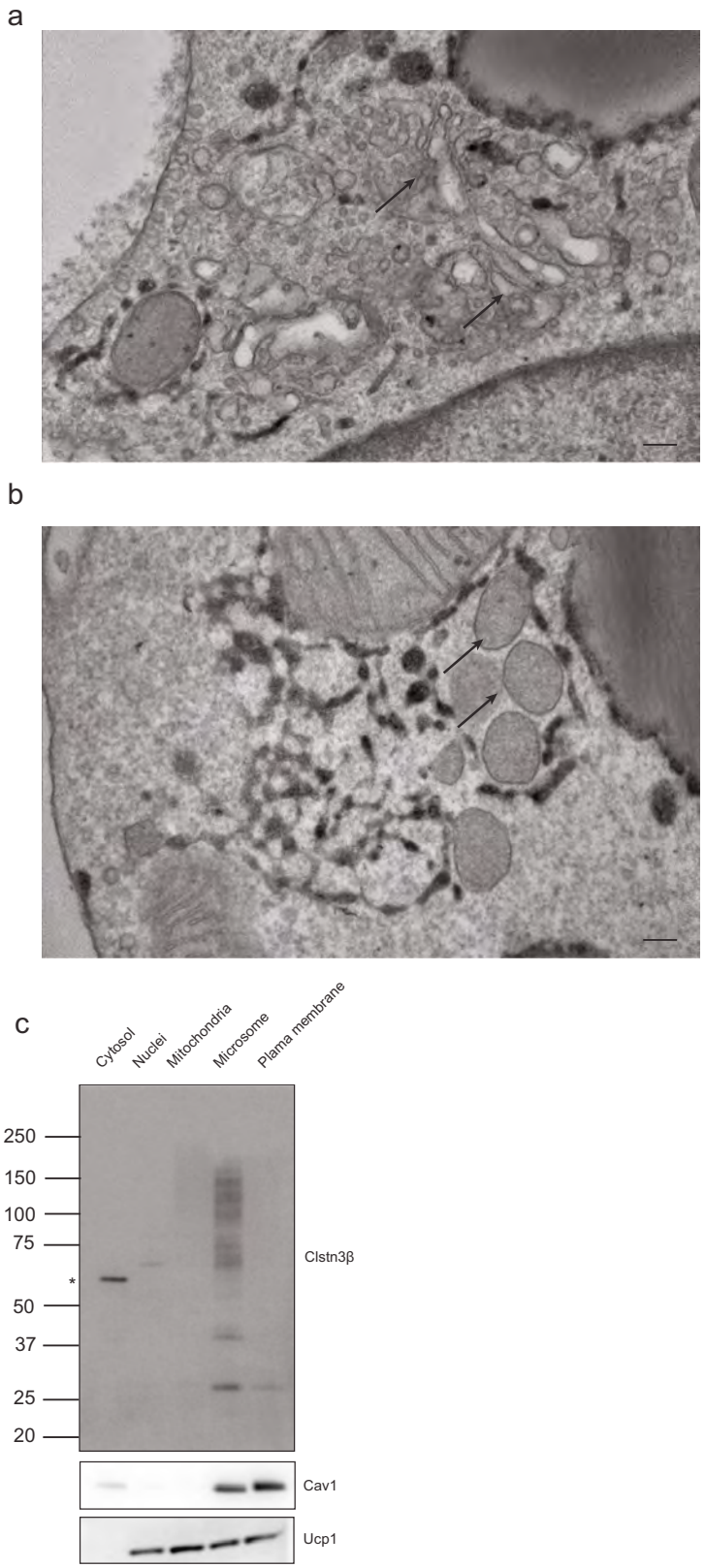

Extended Data Fig. 2 | CLSTN3β localizes to the endoplasmic reticulum. a, **b**, Electron microscopy analysis of primary brown adipocytes that express CLSTN3β–APEX2. In **a**, arrows denote the Golgi apparatus. In **b**, arrows denote peroxisomes. Scale bars, 100 nm. **c**, Western blot analysis of the fractionation pattern CLSTN3β. Asterisk denotes a nonspecific band. For gel source data, see Supplementary Fig. 1.

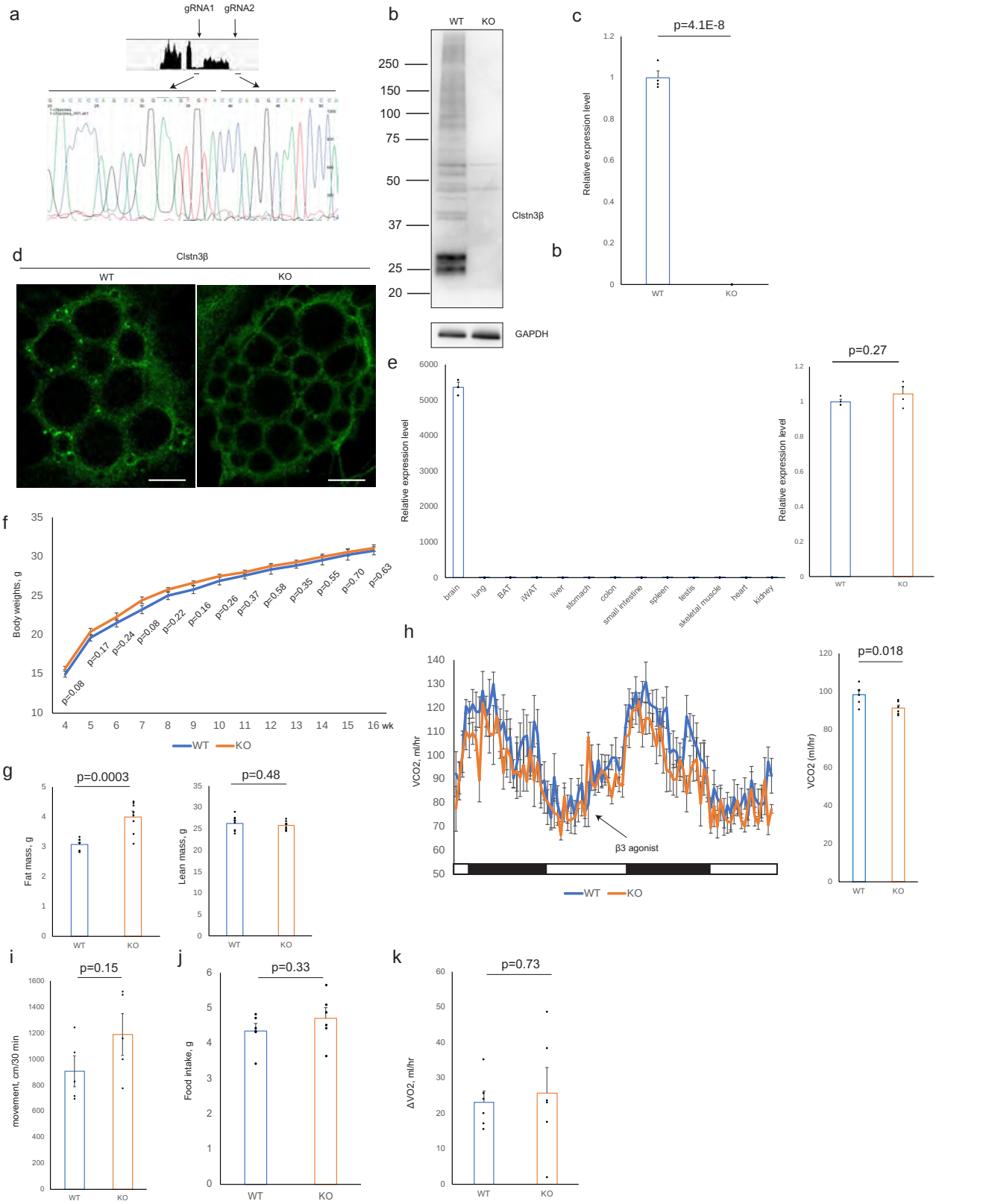

Extended Data Fig. 3 | Ablation of *Clstn3b* impairs adipose thermogenesis. a–d, Sanger sequencing (**a**), western blot (**b**), quantitative PCR (**c**) ($n = 4$ mice) and immunofluorescence (**d**) confirmation of CRISPR–Cas9 deletion of *Clstn3b*. Scale bars, 10 μm. **e**, Quantitative PCR analysis of *Clstn3* expression in a panel of wild-type mouse tissues, and wild-type and *Clstn3b*-knockout brain ($n = 2$ mice for surveying tissue specificity in wild-type mouse; $n = 3$ mice for wild type and knockout). The primers target the junction between the third and the penultimate exons. **f**, **g**, Body weight curve (**f**) and body composition (**g**) of wild-type and *Clstn3b*-knockout mice on chow diet ($n = 8$ mice). **h**, Rates of CO_2 production from indirect calorimetry analysis of wild-type and *Clstn3b*-knockout mice ($n = 6$ mice). **i**, **j**, Movement (**i**) and daily food intake (**j**) of wild-type and *Clstn3b*-knockout mice in metabolic chambers ($n = 6$ mice). **k**, Oxygen consumption response to acute β3 agonist injection, of wild-type and *Clstn3b*-knockout mice ($n = 6$ mice). All data are mean ± s.e.m. Statistical significance was calculated by unpaired Student's two-sided *t*-test.

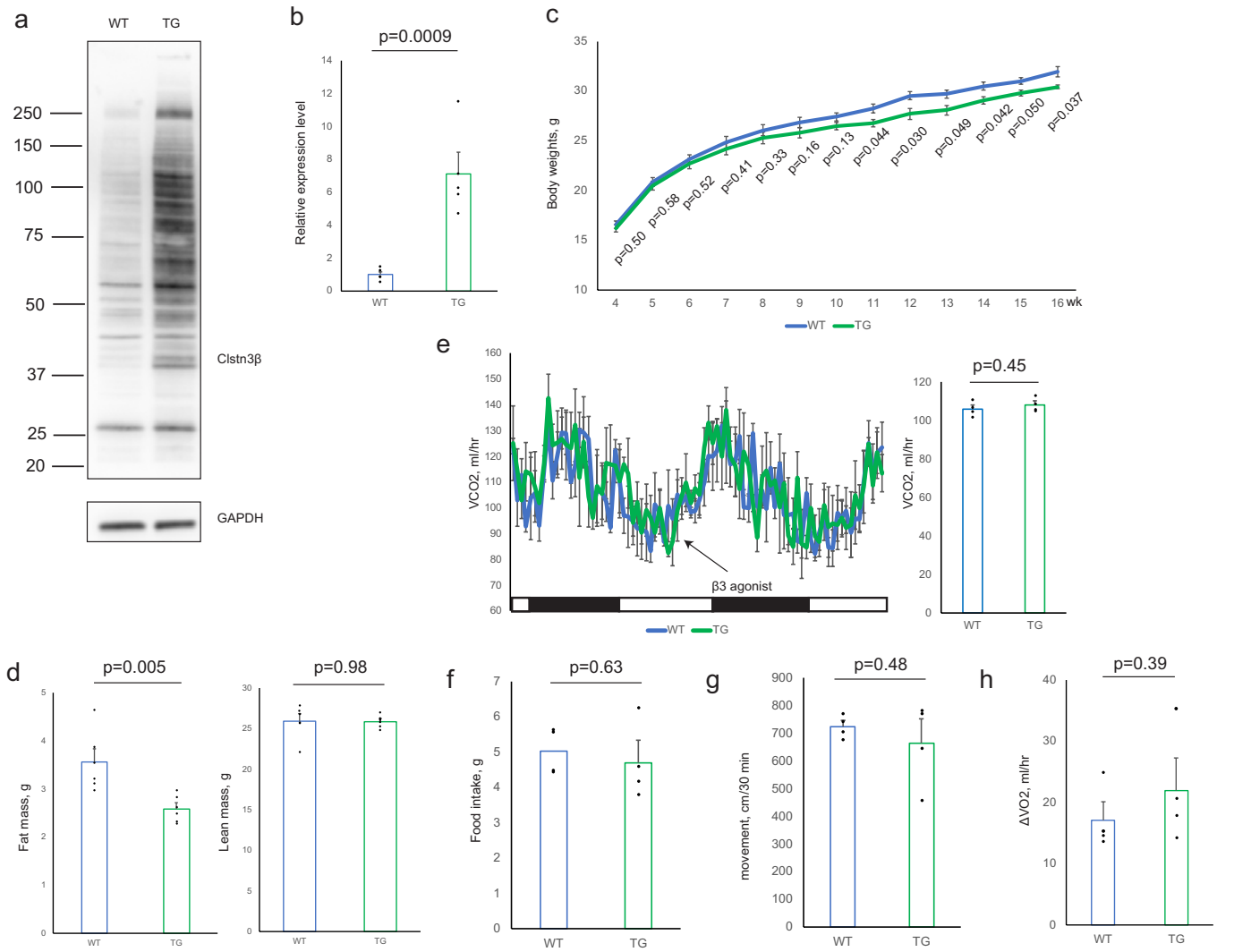

Extended Data Fig. 4 | Transgenic expression of *Clstn3b* increases adipose thermogenesis. a, **b**, Western blot (**a**) and quantitative PCR (**b**) confirmation of transgenic overexpression of CLSTN3β in BAT ($n = 5$ mice). **c**, **d**, Body-weight curve (**c**) and body composition (**d**) of wild-type and *Clstn3b*-transgenic mice on chow diet ($n = 6$ mice). **e**, Rates of CO_2 production from indirect calorimetry analysis of wild-type and *Clstn3b*-transgenic mice ($n = 4$ mice). **f**, **g**, Movement (**f**) and daily food intake (**g**) of wild-type and *Clstn3b*-transgenic mice in metabolic chambers ($n = 4$ mice). **h**, Oxygen consumption response to acute β3 agonist injection of wild-type and *Clstn3b*-transgenic mice ($n = 4$ mice). All data are mean ± s.e.m. Statistical significance was calculated by unpaired Student's two-sided *t*-test.

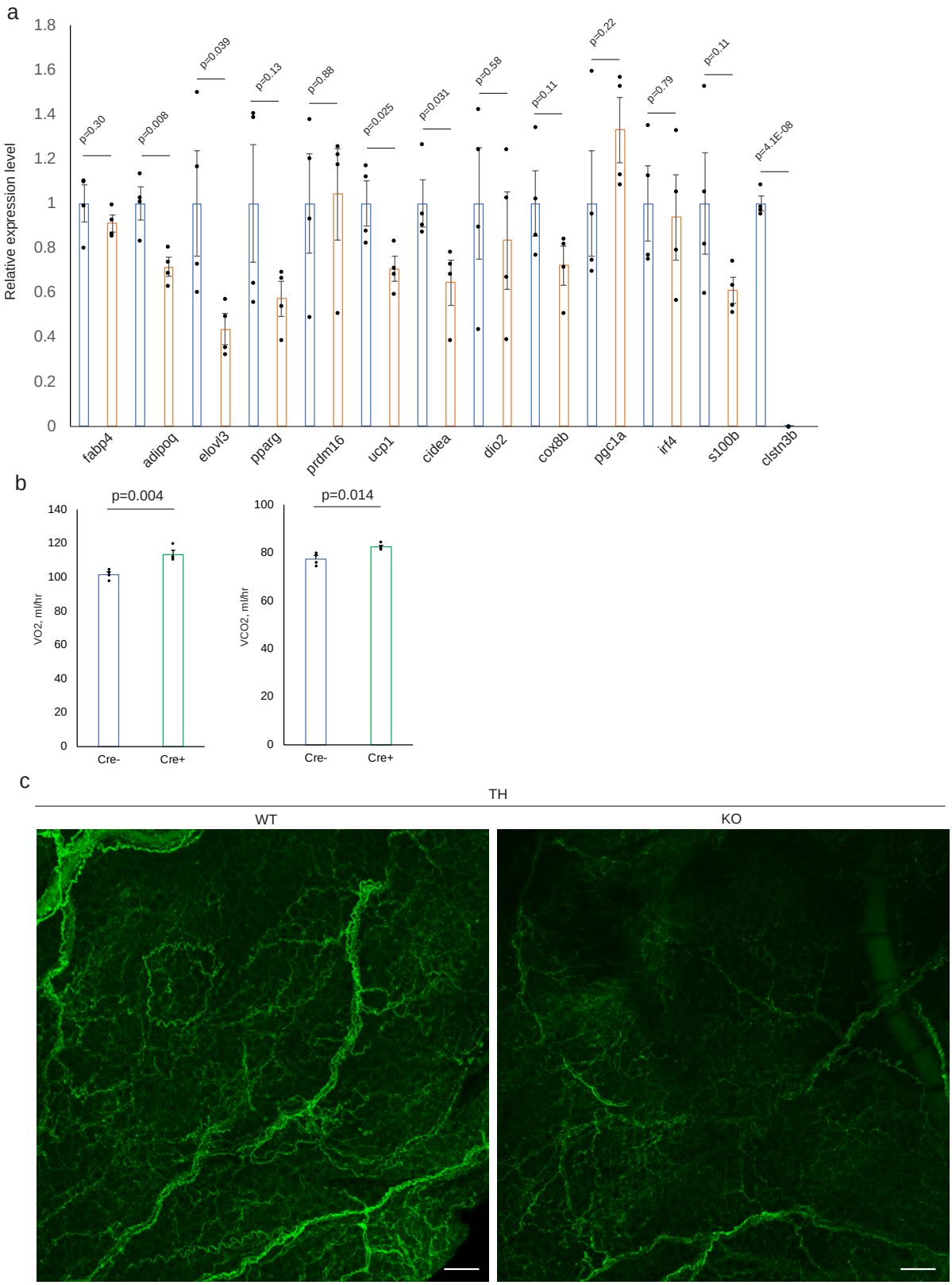

Extended Data Fig. 5 | CLSTN3β increases sympathetic innervation of thermogenic adipose tissue. a, Gene expression analysis of wild-type and *Clstn3b*-knockout BAT upon 5 h of acute cold exposure, following mice being pre-acclimatized to thermoneutrality ($n = 4$ mice). Blue, wild-type; orange, knockout. **b**, Indirect calorimetry analysis of *Clstn3b*-knockout mice with or without *Adipoq-cre*, receiving AAV-DIO-Clstn3b injection ($n = 4$ mice). **c**, Whole-mount tyrosine hydroxylase staining of the inguinal region of the posterior subcutaneous WAT from wild-type and *Clstn3b*-knockout mice, acclimatized at 4 °C for 1 week. Scale bars, 50 μm. All data are mean ± s.e.m. Statistical significance was calculated by unpaired Student's two-sided *t*-test.

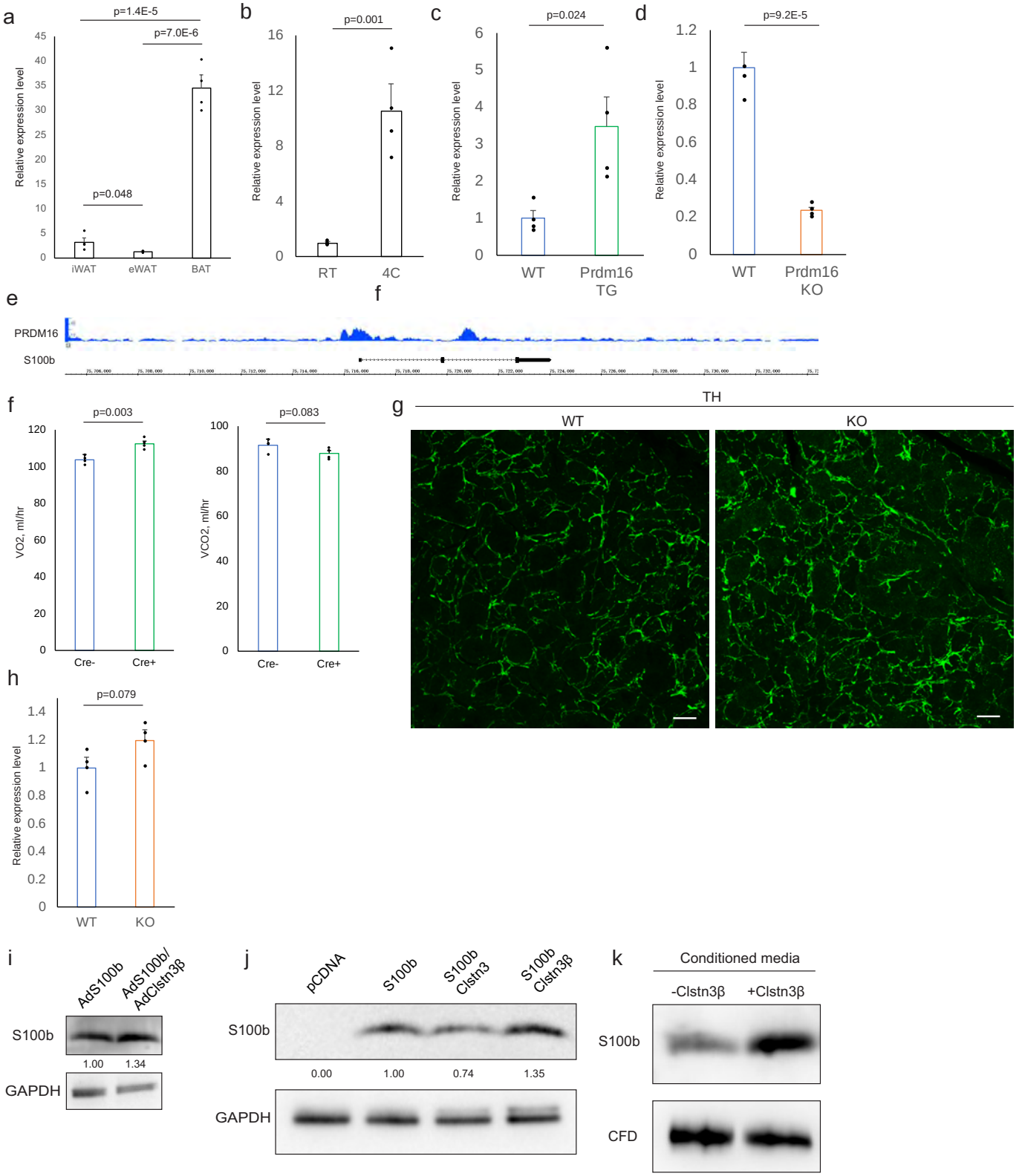

Extended Data Fig. 6 | See next page for caption.

Extended Data Fig. 6 | CLSTN3β promotes secretion of S100b, an adipocyte-derived neurotrophic factor. a, **b**, Quantitative PCR analysis of S100b expression in various fat depots (**a**) and in inguinal subcutaneous WAT (**b**), from mice acclimatized to room temperature or 4 °C ($n = 4$ mice). **c**, Quantitative PCR analysis of S100b expression in control or *Prdm16*-transgenic inguinal subcutaneous WAT ($n = 4$ mice). **d**, Quantitative PCR analysis of S100b expression in control or *Prdm16*-knockout inguinal subcutaneous WAT ($n = 4$ mice). **e**, PRDM16 ChIP–seq showing binding at the *S100b* locus. **f**, Indirect calorimetry analysis of *Clstn3b*-knockout mice with or without *Adipoq-cre*, receiving AAV-DIO-S100b injection ($n = 4$ mice). **g**, Tyrosine hydroxylase immunostaining of salivary gland from wild-type and *S100b*-knockout mice. **h**, Quantitative PCR analysis of S100b expression in wild-type and *Clstn3b*-knockout BAT from mice housed at room temperature ($n = 4$ mice). Note that this is a different housing condition from that used for experiments in Extended Data Fig. 5a. **i**, Western blot analysis of intracellular level of S100b in *Clstn3b*-knockout brown adipocytes that express S100b alone, or co-expressing S100b with CLSTN3β. **j**, Western blot analysis of S100b protein level in HEK293T cells transfected with various constructs as indicated. **k**, Western blot analysis of S100b and complement factor D secretion from HEK293T cells co-transfected with or without CLSTN3β. All data are mean ± s.e.m. Statistical significance was calculated by unpaired Student's two-sided *t*-test.

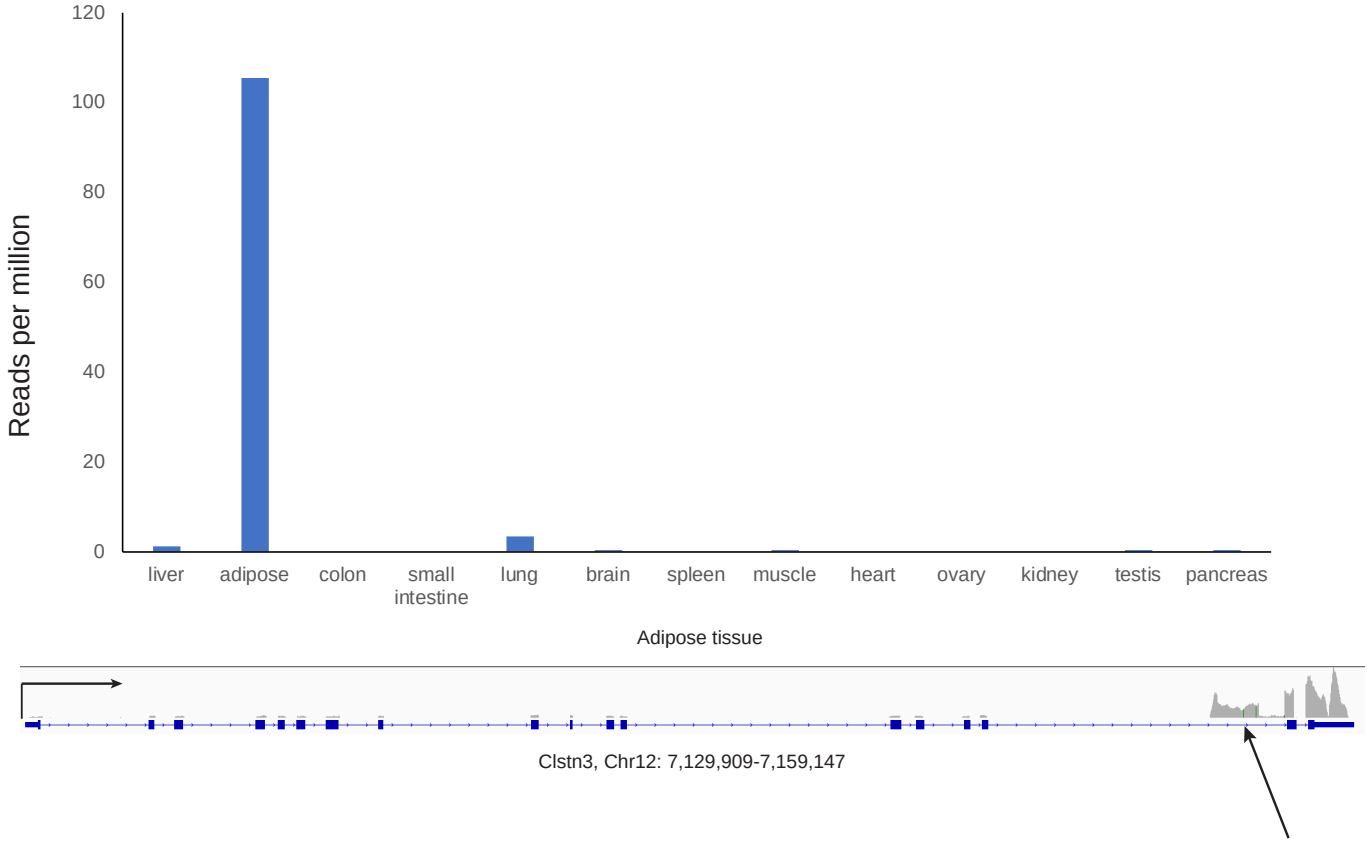

Extended Data Fig. 7 | *Clstn3b* is specifically expressed in human adipose tissue. RNA sequencing in human tissues that shows adipose-specific expression of *Clstn3b*. RNA sequencing of 13 human tissue types was analysed for reads that uniquely map to the *Clstn3b*-specific exon.

nature research

Corresponding author(s): Bruce Spiegelman

Last updated by author(s): Mar 23, 2019

Reporting Summary

Nature Research wishes to improve the reproducibility of the work that we publish. This form provides structure for consistency and transparency in reporting. For further information on Nature Research policies, see Authors & Referees and the Editorial Policy Checklist.

Statistics

For all statistical analyses, confirm that the following items are present in the figure legend, table legend, main text, or Methods section.

n/a	Confirmed	
☐	☒	The exact sample size (*n*) for each experimental group/condition, given as a discrete number and unit of measurement
☐	☒	A statement on whether measurements were taken from distinct samples or whether the same sample was measured repeatedly
☐	☒	The statistical test(s) used AND whether they are one- or two-sided *Only common tests should be described solely by name; describe more complex techniques in the Methods section.*
☒	☐	A description of all covariates tested
☒	☐	A description of any assumptions or corrections, such as tests of normality and adjustment for multiple comparisons
☐	☒	A full description of the statistical parameters including central tendency (e.g. means) or other basic estimates (e.g. regression coefficient) AND variation (e.g. standard deviation) or associated estimates of uncertainty (e.g. confidence intervals)
☐	☒	For null hypothesis testing, the test statistic (e.g. *F*, *t*, *r*) with confidence intervals, effect sizes, degrees of freedom and *P* value noted *Give P values as exact values whenever suitable.*
☒	☐	For Bayesian analysis, information on the choice of priors and Markov chain Monte Carlo settings
☒	☐	For hierarchical and complex designs, identification of the appropriate level for tests and full reporting of outcomes
☒	☐	Estimates of effect sizes (e.g. Cohen's *d*, Pearson's *r*), indicating how they were calculated

Our web collection on statistics for biologists contains articles on many of the points above.

Software and code

Policy information about availability of computer code

Data collection	Oxymax 5.0 for CLAMS; NIS element for confocal imaging; LAS-3000 Imaging System from Fuji for Western blot; Applied Biosystems 7500 for qPCR.
Data analysis	Imaris 8.4 and Image J 1.52 for imaging analysis; Excel 2016 for statistical analysis. Integrated genome viewer for sequencing data

For manuscripts utilizing custom algorithms or software that are central to the research but not yet described in published literature, software must be made available to editors/reviewers. We strongly encourage code deposition in a community repository (e.g. GitHub). See the Nature Research guidelines for submitting code & software for further information.

Data

Policy information about availability of data

All manuscripts must include a data availability statement. This statement should provide the following information, where applicable:

- Accession codes, unique identifiers, or web links for publicly available datasets
- A list of figures that have associated raw data
- A description of any restrictions on data availability

All data will be available in publicly available datasets or upon request to the Spiegelman laboratory after publication.

Field-specific reporting

Please select the one below that is the best fit for your research. If you are not sure, read the appropriate sections before making your selection.

☒ Life sciences ☐ Behavioural & social sciences ☐ Ecological, evolutionary & environmental sciences

Life sciences study design

All studies must disclose on these points even when the disclosure is negative.

Sample size	No sample size pre-determination was performed. Samples size was chosen based on previous experience that would be sufficient to achieve statistical signifcance.
Data exclusions	No data were excluded.
Replication	All experiments have been successfully repeated with similar results for at least three times.
Randomization	Mice were grouped based on genotype and therefore no randomization was required for this study.
Blinding	Imaging investigator was blinded during data analysis.

Reporting for specific materials, systems and methods

We require information from authors about some types of materials, experimental systems and methods used in many studies. Here, indicate whether each material, system or method listed is relevant to your study. If you are not sure if a list item applies to your research, read the appropriate section before selecting a response.

Materials & experimental systems

n/a	Involved in the study
☐	☒ Antibodies
☐	☒ Eukaryotic cell lines
☒	☐ Palaeontology
☐	☒ Animals and other organisms
☒	☐ Human research participants
☒	☐ Clinical data

Methods

n/a	Involved in the study
☐	☒ ChIP-seq
☒	☐ Flow cytometry
☒	☐ MRI-based neuroimaging

Antibodies

Antibodies used	Clstn3β antibody was generated at Covance. S100b antibody, Abcam, ab51642. TH antibody, EMD Millipore, AB1542. TUBB3 antibody, Abcam, ab52623. KDEL antibody, Abcam, ab50601. Ucp1 antibody, Abcam, ab10983. Cav1 antibody, Abcam, ab192869. GAPDH, Abcam, ab9485. FLAG antibody, Sigma-Aldrich, F1804. Cfd antibody, Abcam, ab213177. mCherry antibody, ThermoFisher M11217; cfos antibody, EMD Millipore, ABE457. Donkey anti sheep Alexa Fluor 488 antibody, ThermoFisher, A-11015. Goat anti rabbit Alexa Fluor 617 antibody, ThermoFisher, A-27040. Goat anti rat Alex Fluor 488 antibody, ThermoFisher, A-11006; Donkey anti rat Alex Fluor 594 antibody, ThermoFisher, A21209; Donkey anti rabbit Alex Fluor 488 antibody, ThermoFisher, A21206.
Validation	Clstn3β antibody was validated by both KO and transgenic tissue samples. All commercially available antibodies were validated for detecting mouse proteins by immunostaining or Western blot by the manufacturers.

Eukaryotic cell lines

Policy information about cell lines

Cell line source(s)	HEK293T from ATCC.
Authentication	This cell line was maintained in the Spiegelman and not specifically authenticated for this study.
Mycoplasma contamination	The cell line was tested negative for mycoplasma.
Commonly misidentified lines (See ICLAC register)	No commonly misidentified lines were used.

Animals and other organisms

Policy information about studies involving animals; ARRIVE guidelines recommended for reporting animal research

Laboratory animals	Mus musculus. Clstn3β KO, Clstn3β transgenic, adiponetcin-cre, and S100b KO mice were all on the C57Bl/6 background. Vlug3-ires-cre line had a mixed background. Male mice at age 8-12 weeks were used for experiments.

Wild animals	This study did not involve wild animals.
Field-collected samples	This study did not involve field-collected samples.
Ethics oversight	Beth Israel Deaconess Medical Center IACUC.

Note that full information on the approval of the study protocol must also be provided in the manuscript.

ChIP-seq

Data deposition

☒ Confirm that both raw and final processed data have been deposited in a public database such as GEO.

☐ Confirm that you have deposited or provided access to graph files (e.g. BED files) for the called peaks.

Data access links *May remain private before publication.*	BAT H3K4me3 and H3K27Ac are from ENCODE database. Accession code: ENCSR000CFB for H3K4me3 and ENCSR000CEZ for H3K27Ac. All other datasets are available at NIH SRA under the accession code PRJNA526243.
Files in database submission	BAT_H3K4me1_rep1.bam BAT_H3K4me1_rep2.bam BAT_H3K4me2_rep1.bam BAT_H3K4me2_rep2.bam BAT_H3K79me3_rep1.bam BAT_H3K79me3_rep2.bam BAT_LSD1.bam BAT_PPARG.bam
Genome browser session (e.g. UCSC)	N/A.

Methodology

Replicates	Two replicates for each sample for Histone markers. One replicate for LSD1 and PPARG.
Sequencing depth	30-50 million reads per sample
Antibodies	H3K4me1, EMD Millipore 07-436; H3K4me2, EMD Millipore 07-030; H3K79me3, Abcam ab2621; PPARG, SantaCruz, H-100; LSD1, Abcam, ab17721
Peak calling parameters	This study does not involve peak calling but only concerns reads distribution at a specific locus.
Data quality	Not relevant for this study.
Software	CLC Genomics Workbench 11.